

Zc3h13/Flacc is required for adenosine methylation by bridging the mRNA binding factor Rbm15/Spentito to the m⁶A machinery component Wtap/Fl(2)d

Philip Knuckles^{1,2,10}, Tina Lence^{3,10}, Irmgard U. Haussmann^{4,5}, Dominik Jacob⁶, Nastasja Kreim⁷, Sarah H. Carl^{1,9}, Irene Masiello^{3,8}, Tina Hares³, Rodrigo Villaseñor^{1,2,11}, Daniel Hess¹, Miguel A. Andrade-Navarro³, Marco Biggiogera⁸, Marc Helm⁶, Matthias Soller⁴, Marc Bühler^{1,2,12} and Jean-Yves Roignant^{3,12}

(1)Friedrich Miescher Institute for Biomedical Research, Maulbeerstrasse 66, 4058 Basel, Switzerland

(2)University of Basel, Basel, Switzerland

(3)Laboratory of RNA Epigenetics, Institute of Molecular Biology (IMB), Mainz, 55128, Germany

(4)School of Life Science, Faculty of Health and Life Sciences, Coventry University, Coventry CV1 5FB

(5)School of Biosciences, College of Life and Environmental Sciences, University of Birmingham, Edgbaston, Birmingham, B15 2TT, United Kingdom

(6)Institute of Pharmacy and Biochemistry, Johannes Gutenberg University of Mainz, 55128 Mainz, Germany

(7)Genomic core facility, Institute of Molecular Biology (IMB), Mainz, 55128, Germany

(8)Laboratory of Cell Biology and Neurobiology, Department of Animal Biology, University of Pavia, Pavia, Italy.

(9)Swiss Institute of Bioinformatics, Basel, Switzerland

(10) These authors contributed equally to this work

(11) Current address: Department of Molecular Mechanisms of Disease, University of Zurich, Winterthurstrasse 190, 8057 Zürich, Switzerland

(12) Correspondence to: marc.buehler@fmi.ch and j.roignant@imb-mainz.de

Running title: Zc3h13/Flacc is required for m⁶A biogenesis

Key words: Zc3h13, Flacc, m⁶A, methyltransferase complex, RNA modifications, sex determination

Abstract

N⁶-methyladenosine (m⁶A) is the most abundant mRNA modification in eukaryotes, playing crucial roles in multiple biological processes. m⁶A is catalyzed by the activity of Mettl3, which depends on additional proteins whose precise functions remain poorly understood. Here we identified Flacc/Zc3h13 as a novel interactor of m⁶A methyltransferase complex components in *Drosophila* and mouse. Like other components of this complex, Flacc controls m⁶A levels and is involved in sex determination in *Drosophila*. We demonstrate that Flacc promotes m⁶A deposition by bridging Fl(2)d to the mRNA binding factor Nito. Altogether, our work advances our molecular understanding of conservation and regulation of the m⁶A machinery.

Introduction

In the past years N^6 -methyladenosine RNA (m^6A) has emerged as an abundant and dynamically regulated modification throughout the transcriptome (Dominissini et al. 2012; Meyer et al. 2012). m^6A affects almost every stage of mRNA metabolism and its absence is associated with various defects in meiosis, embryonic stem cell differentiation, DNA repair, circadian rhythm, neurogenesis, dosage compensation and sex determination (for a recent review see (Roignant and Soller 2017; Zhang et al. 2017)). Alteration of m^6A levels also promotes glioblastoma progression and is linked to poor prognosis in myeloid leukemia (Yu et al. 2012; Cui et al. 2017; Kwok et al. 2017; Zhang et al. 2017).

Formation of m^6A is catalyzed by the activity of methyltransferase like 3 (METTL3, also called MT-A70) (Bokar et al. 1997), which physically interacts with methyltransferase like 14 (METTL14) (Liu et al. 2014; Ping et al. 2014; Schwartz et al. 2014; Wang et al. 2014), Wilms tumor 1-associated protein (WTAP) (Zhong et al. 2008; Agarwala et al. 2012), Vir-like m^6A methyltransferase associated (KIAA1429/VIRMA) (Schwartz et al. 2014), and RNA Binding Motif 15 (RBM15) and its paralogue RBM15B (Patil et al. 2016b). *Drosophila* has corresponding homologues Mettl3, Mettl14, Fl(2)d, Virilizer (Vir), and Spenito (Nito) (Lence et al. 2017). Recent crystal structural studies investigated the molecular activities of the two predicted methyltransferases METTL3 and METTL14 (Sledz and Jinek 2016; Wang et al. 2016a; Wang et al. 2016b). Only METTL3 was shown to contain the catalytic activity and to form a stable heterodimer with METTL14, which was required to enhance METTL3 enzymatic activity by binding substrate RNA and by positioning the methyl group for transfer to adenosine. Besides, WTAP (Fl(2)d) ensures the stability and localisation of the heterodimer to nuclear

speckles (Ping et al. 2014; Lence et al. 2016). VIRMA (Vir) is essential for m⁶A deposition but its molecular function is currently unknown. Lastly, RBM15 and RBM15B (Nito) have been suggested to recruit the methyltransferase complex to its target transcripts via direct binding to U-rich sequences on mRNA. In humans this function is important to control m⁶A promoted X-chromosome inactivation via *XIST*-mediated transcriptional repression (Patil et al. 2016b). In *Drosophila*, Nito promotes m⁶A function in the sex determination and dosage compensation pathways (Lence et al. 2016).

To date it is unknown how Nito in *Drosophila* interacts with other members of the methyltransferase writer complex to ensure their recruitment to mRNA targets. Although in human cells RBM15/15B were reported to interact with METTL3 in a WTAP-dependent manner (Patil et al. 2016a), it is unclear whether this interaction is conserved in other organisms. In order to address these questions we have performed interactome analyses from *Mus musculus* and *Drosophila melanogaster* cell extracts using Rbm15 and Nito as bait, respectively. We identified mouse zinc finger CCCH domain-containing protein 13 (Zc3h13) and its fly homolog CG7358, which we named Fl(2)d Associated Complex Component (Flacc), as novel interactors of the m⁶A writer machinery. Lack of these proteins dramatically reduces m⁶A levels in both organisms. Consistent with the role of m⁶A in sex determination in *Drosophila*, Flacc depletion results in aberrant splicing of *Sex lethal* (*Sxl*) and leads to transformations of female into male-like structures. Moreover, we demonstrate that Flacc interacts with Nito and Fl(2)d, and serves as an adaptor between these two proteins, thereby stabilizing the complex and promoting m⁶A deposition on mRNAs.

Results

1- Zc3h13 interacts with the m⁶A machinery

In our recent work we identified Nito as a novel interactor of the m⁶A methyltransferase complex (Lence et al. 2016). Because the role of the mouse Nito homolog Rbm15 in m⁶A deposition appears to be evolutionarily conserved (Patil et al. 2016), we sought to identify interaction partners to obtain further insights into Rbm15's function. To this end, we tagged endogenous Rbm15 with the FLAG-Avi tag using CRISPR-Cas9 genome editing in mouse embryonic stem cells (mESCs) that express the bacterial *BirA* ligase (Flemr and Buhler 2015) (Supplemental Fig. S1A and B). Subsequently, we performed tandem affinity purification coupled to liquid chromatography and mass spectrometry (TAP-LC-MS). We found that Rbm15 co-purifies with Wtap, Virma, and Hakai (Fig.1A) under stringent conditions (350mM NaCl), demonstrating that these proteins stably interact with each other. Hakai was recently found to interact with other subunits of the m⁶A methyltransferase complex in plants (Ruzicka et al. 2017). Interestingly, we also observed Zc3h13 amongst the top hits. Although it was reported to interact with WTAP in human cells, it has previously not been linked to adenosine methylation (Horiuchi et al. 2013; Wan et al. 2015).

Previous work suggested that the interaction of the heterodimer Mettl3/14 with Wtap, Virma and Rbm15 is important to guide the methylation complex to its targets and correctly methylate mRNA (Ping et al. 2014; Schwartz et al. 2014; Patil et al. 2016b). To test whether the Zc3h13 containing protein complex described above interacts with Mettl3/14 in mouse, we also endogenously tagged Mettl3 with the FLAG-Avi tag in mESCs (Supplemental Fig. S1A and B) and performed TAP-LC-MS. Consistent with previous reports, we found that Mettl3 co-purifies with Mettl14, Wtap, Virma, Rbm15 and Hakai. (Fig. 1B and Supplemental Fig. S2A). Importantly, we also recovered

peptides from Zc3h13 (Fig. 1B and Supplemental Fig. S2A). Whereas these interactions resisted 350mM NaCl, only the Mettl3/Mettl14 interaction remained at 500 mM NaCl (Fig. 1B). These results indicate the existence of two stable protein complexes (Mettl3/Mettl14 and Rbm15/Zc3h13/Wtap/Virma/Hakai), which we refer to as m⁶A-METTL Complex “MAC” and m⁶A-METTL Associated Complex “MACOM”, respectively.

To gain further insight into the relative amounts of MAC to MACOM we performed iBAQ analysis on TAP-LC-MS data from endogenously tagged Mettl3. We could observe comparable stoichiometry between the bait (Mettl3) and Mettl14. In contrast, WTAP and other MACOM components were less than 1% abundant compared to Mettl3 and Mettl14 (Supplemental Fig. S2B), an observation that we interpret as a sign of a weak and/or short-lived interaction. Alternatively, the abundance of MAC bound to MACOM could be very scarce relative to the level of each independent complex. Regardless of the precise mechanism, because components of both complexes are required to install m⁶A, we propose that MAC and MACOM interact with each other in order to deposit the methylation.

2- The *Drosophila* Zc3h13 homolog Flacc interacts with components of the m⁶A methyltransferase complex

To address whether Nito interacts with the same set of proteins that we identified in mouse, we took a very similar approach as above using extracts from *Drosophila* S2R+ cells. To find Nito interacting partners we used stable isotope labeling of amino acids in cell culture (SILAC)-based quantitative proteomics. A Myc-tagged version of Nito was used to perform co-immunoprecipitation experiments from S2R+ cells. In total, we identified 40 factors that showed more than 1.5-fold enrichment in the Nito-Myc

precipitate in comparison to control cells transfected with Myc alone (Fig. 1C and Supplemental Table 1). In agreement with mouse Rbm15 proteomic analysis, the homolog of Wtap in *Drosophila*, Fl(2)d, was among the top candidates. We also found the previously reported m⁶A writers Vir and Hakai (refer to Fig. 1F for *Mus musculus* and *Drosophila melanogaster* nomenclature of m⁶A factors). We observed an overall enrichment for mRNA binding proteins (Fig. 1D) and, importantly, Flacc, which is the closest homolog of Zc3h13. To confirm the interaction of this protein with Nito, we generated tagged proteins and performed co-immunoprecipitation assays. These experiments confirmed that Flacc interacts with Nito, and that this occurs in an RNA-independent manner (Fig. 1E). To verify that Flacc interacts with other components of the m⁶A methyltransferase complex, we immunoprecipitated Flacc-Myc and tested for the presence of Vir and Fl(2)d. As shown in Supplemental Fig. S3A, B, Flacc interacts with both proteins independently of RNA, indicating that it might be a novel regulator of the m⁶A pathway. In contrast to mouse Zc3h13 (see below), however, Flacc does not contain a zinc finger motif (Supplemental Fig. S4).

3- Zc3h13/Flacc regulates the m⁶A pathway

To test whether Zc3h13 is necessary for adenosine methylation in mice, we measured global m⁶A levels by LC-MS/MS in *Zc3h13* knock out (KO) mESCs (Supplemental Fig. S1C). We found a 90% reduction of m⁶A, similar to isogenic *Mettl3* KO mESCs (Fig. 2A). Consistent with a global reduction in m⁶A levels, *Zc3h13* KO cells displayed a drastic change in morphology, reminiscent to *Mettl3* KO, with loss of dome-shaped colony formation and an overall increase in cell size (data not shown). In addition, we performed m⁶A RNA-immunoprecipitation coupled to deep sequencing (m⁶A-RIP-seq) on oligo-dT selected mRNA from wild type, *Mettl3*^{-/-}, and *Zc3h13*^{-/-} mESCs. As

observed with *Mettl3* KO cells, ablation of *Zc3h13* resulted in a drastic reduction of m⁶A enrichment, particularly at the 3' end of target mRNAs (Fig. 2B and C). Hence, we conclude that *Zc3h13* is essential for m⁶A installation in mouse embryonic stem cells. To investigate evolutionary conservation of this activity in *Drosophila*, we quantified m⁶A levels using LC-MS/MS analysis upon Flacc depletion in *Drosophila* S2R+ cells. Similar to the reduction observed upon knock down of other m⁶A components, depletion of Flacc also resulted in strongly reduced m⁶A levels (Fig. 2D and Supplemental Fig. S5A). This was not due to an indirect effect on expression of other components of the methyltransferase complex (Fig. S5B-D). In agreement with decreased m⁶A levels, we found that binding of the reader protein Ythdc1 to its target transcripts was reduced in the absence of Flacc (Fig. 2E). Together, these results demonstrate that *Zc3h13* and its *Drosophila* orthologue Flacc are novel and essential components of the m⁶A pathways in mouse and flies.

4- Flacc is required for pre-mRNA splicing

To further corroborate Flacc as a *bona fide* m⁶A writer, we tested whether it was required to control m⁶A-splicing related events. As previously reported, splicing of several transcripts, including *AldhIII*, *Dsp1*, and *Hairless* is dependent on the m⁶A pathway (Lence et al. 2016). Remarkably, depletion of Flacc affected all those transcripts (Fig. 2F and Supplemental Fig. S5E). We next expanded this analysis to a transcriptome wide level, which revealed that depletion of Flacc in S2R+ cells leads to changes in gene expression and splicing that substantially overlap with changes observed upon knock down of other m⁶A writers (Fig. 3A, supplemental Fig. S6A). In particular, the Flacc-depleted transcriptome clusters very closely with Fl(2)d- and Vir-depleted transcriptomes (Fig. 3B). Notably, Nito depletion induced greater changes, and poorly

clustered with the others, suggesting that Nito might be pleiotropic. Regardless of Nito's potential role in other pathways, common mis-regulated transcripts among components of the MACOM complex are larger than the average transcript size (Figure 3C, P value \Rightarrow) and are significantly methylated (61.5%; P value \leftarrow) (Fig 3D). Importantly, differentially expressed genes generally change in the same direction upon the different KD, confirming that MACOM components belong to the same complex and share similar functions (Fig 3E). We noticed that common up-regulated genes tend to be larger than average expressed gene ($p=2.9e-40$) and more methylated compared to down-regulated ones (78.2%, $p=6.1e-31$ vs. 44.5%, $p=0.086$) (Fig. 3C, D). Up regulated genes were enriched for processes involved in embryonic development as well as epithelial cell differentiation and migration (Fig. 3F). Thus, it is possible that down-regulated genes, which are mostly enriched for metabolic processes, are affected indirectly (Fig. 3F).

We next performed similar analysis with respect to splicing changes. We found that knock down of each of the known m⁶A writer components, including Flacc, resulted in an increase of both alternative 5' splice site usage and intron retention (Supplemental Fig. S6A, B). Moreover, common mis-spliced transcripts upon KD of MACOM components are highly methylated (82.2%, $p=1.3e-8$), show similar splicing defects, and are enriched for neuronal processes, which is consistent with our previous findings (Lence et al. 2016) (Supplemental Fig. S6C-E). Of note, KD of Mettl3/Mettl14 generally produces less effect compared to KD of MACOM components. This may be explained by residual m⁶A activity upon KD of the methyltransferases. Alternatively, MACOM components may have additional function(s) beyond m⁶A activity (see also discussion).

5- Flacc subcellular localization and expression through development

To further investigate the role of Flacc in *Drosophila*, we examined its subcellular localization as well as its developmental expression profile. We observed that Flacc is strictly localized in the nucleus in S2R+ cells (Supplemental Fig. S7A) and that its transcript is broadly expressed during embryogenesis, but shows enrichment in the neuroectoderm (Supplemental Fig. S7B). Overall, *flacc* mRNA follows the same distribution as transcripts of other subunits of the methyltransferase complex (Lence et al. 2016) and as m⁶A levels in mRNA. An exception is the stage of maternal to zygotic transition (2 hours post fertilization) where a boost of *flacc* expression is observed, while m⁶A is rapidly decreasing (Supplemental Fig. S7C), suggesting that Flacc might have an additional function in early embryogenesis.

6- Flacc is required for sex determination and dosage compensation via *Sxl* alternative splicing

Components of the m⁶A machinery were previously shown to affect sex determination and dosage compensation in *Drosophila* via the control of *Sxl* alternative splicing (Hausmann et al. 2016; Lence et al. 2016; Kan et al. 2017a). To address whether Flacc bears similar functions, we depleted its products by expressing its corresponding double-stranded RNA (dsRNA) in both the legs and genital discs using the *dome*-GAL4 driver. Strikingly, these females displayed clear transformations into male structures, as previously shown for Nito (Fig. 4A) (Yan and Perrimon 2015). This is illustrated by the appearance of sex combs in the forelegs of females that were depleted for Flacc. The phenotype is observed in about 20% of females examined (Fig. 4B). Using a dsRNA that targets a distinct region of *flacc* (GD35212), the penetrance was even increased to all female escapers. Furthermore, typical female external structures, such as vaginal bristles,

were absent on the same individuals (Fig. 4A). Altogether, these data indicate that Flacc plays a major role in the control of sex determination in flies.

To address how Flacc affects sex determination, we tested whether alternative splicing of *Sxl*, the master regulator of sex determination and dosage compensation, was affected. RNA extracts from fly heads, depleted by RNAi for Fl(2)d, Nito, or Flacc, were subjected to reverse transcription followed by PCR using primers spanning the common exons 2 and 4. While the male specific exon 3 is absent in control female heads, it was clearly included upon loss of components of the m⁶A machinery, including Flacc (Fig. 4C). This experiment indicates that Flacc regulates sex determination and dosage compensation via *Sxl* alternative splicing, as previously shown for other m⁶A writers.

To confirm the effect of Flacc on sex determination via *Sxl* alternative splicing observed when using RNAi, we analyzed a lethal *flacc* mutant allele harboring a stop codon at amino acid 730 (Fig. 4D). Reducing one copy of m⁶A components (*Mettl3*, *Mettl14*, *fl(2)d*, *vir*, *nito* or *Ythdc1*) in a sensitized background (heterozygous for *Sxl* and *daughterless*) significantly alters female viability (Fig. 4E). We previously showed for the *Mettl3* allele that this is due to activation of dosage compensation in females (Hausmann et al. 2016). Consistent with its role in N⁶-adenosine methylation, we found that removing one copy of the *flacc* allele results in female lethality (Fig. 4E). Likewise, the female-lethal single amino acid substitution allele *vir2F* interferes with *Sxl* recruitment, resulting in impaired *Sxl* auto-regulation and inclusion of the male-specific exon (Hilfiker et al. 1995). We observed that female lethality of these alleles was rescued by *flacc* and *nito* double heterozygosity, further confirming the involvement of Flacc in *Sxl* alternative splicing (Fig. 4F).

7- Zc3h13/Flacc stabilizes Wtap/Fl(2)d - Rbm15/Nito interaction

To obtain insights into the molecular function of Flacc, we investigated interactions between m⁶A writers in the absence of Flacc. We previously found that knock down of Fl(2)d diminishes the interaction between Mettl3 and Mettl14 (Lence et al. 2016). Interestingly, we found that this interaction is not affected upon Flacc knock down (Supplemental Fig. S8A and B). However, we observed that depleting Flacc almost completely abolished the association between Nito and Fl(2)d (Fig. 5A), whereas the interaction between two different isoforms of Fl(2)d and Vir, Nito and Vir, as well as Nito and Mettl3/Mettl14 were not affected (Supplemental Fig. S8C-I). This indicates that Flacc stabilizes the complex and might serve as an adapter that connects the RNA binding protein Nito to Fl(2)d. If this prediction was true, depletion of Flacc should prevent binding of Fl(2)d, but not Nito, to its mRNA targets. To test this hypothesis, we performed RNA immunoprecipitation (RIP) experiments to monitor the binding of these components to well-characterized m⁶A targets in the presence or absence of Flacc. As shown in figure 5B, binding of Fl(2)d to *AldhIII*, *Hairless*, and *Dsp1* mRNA was strongly decreased upon Flacc knock down, whereas Nito binding was only slightly affected. Thus, we conclude that Flacc serves as an adapter between Fl(2)d and the mRNA recruiting factor RBM15/Nito.

To test functional conservation of Flacc, we cloned a human isoform of ZC3H13 and probed for the interaction between Nito and Fl(2)d upon depletion of endogenous Flacc protein in *Drosophila* S2R+ cells. Remarkably, expression of ZC3H13 was sufficient to re-establish the interaction between Nito and Fl(2)d (Fig. 5C and D), even though the two orthologs bear very low sequence similarity at the amino acid level (21% identity). These results hint towards a conserved role of this newly characterized protein in stabilizing interactions within the MACOM complex. To address this more directly, we generated *Zc3h13* KO mESCs that express FLAG-Avi tagged Rbm15 and performed

TAP-LC-MS/MS experiments. Starting both with whole cell extracts or nuclear fractions, Rbm15 interaction with Wtap was markedly reduced (Fig. 6A, B and Supplemental Fig. S9A, B), which is consistent with observations in the fly KD experiments (Nito and Fl(2)d respectively). Furthermore, the reduced interaction was not attributable to a global decrease of Wtap, nor other components of MACOM (Supplemental Fig. 9A). As an alternative approach to test MACOM integrity, we employed a protein fragment complementation assay (Dixon et al. 2016), generating fusion constructs of Rbm15 and Wtap to NanoBiT subunits. The optimal combination of fusions reconstituted luciferase signal when transfected into WT cells (Wtap N-terminally tagged with the small Nanoluciferase subunit and Rbm15 C-terminally tagged with the large Nanoluciferase subunit (Fig. 6C and Supplemental Fig. 9D-F). Relative luciferase signal intensity was strikingly reduced when fusion constructs were transfected in *Zc3h13 KO* but not in *Mettl3 KO*, discarding a secondary effect of global m⁶A loss (Fig. 6C). Taken together, these findings suggest that Zc3h13 acts as an adapter that connects the RNA binding protein Rbm15 to Wtap also in mammals.

Discussion

Our study identified a novel interactor of the m⁶A methyltransferase complex, which is conserved in *Drosophila* and mouse. Its function in the m⁶A pathway is essential in both species as its absence results in dramatic reduction of m⁶A levels. The fact that the human homolog was recently found in interactome studies with WTAP (Horiuchi et al. 2013; Wan et al. 2015), and that it can rescue the interaction between Fl(2)d and Nito in *Drosophila*, suggests that it has a similar role in human cells. Despite this functional conservation, the protein sequence identity amongst different homologs is rather weak (Supplemental Fig. S5). Mouse Zc3h13 contains several additional domains as compared to Flacc. In particular, it differs by the presence of a zinc finger domain, which is present in a common ancestor but was lost in dipterian (Supplemental Fig. S5). Other species like *Ciona intestinalis* also lack the zinc finger motif. In addition, the zinc finger motif can be found in two variants across evolution, one short and one long. As zinc finger motifs are commonly involved in nucleic acid binding or protein-protein interactions, it will be interesting to address the functional importance of this domain when present in the protein. Of note, Zc3h13 appears completely absent in nematodes, as it is also the case for Mettl3 (Dezi et al. 2016), possibly indicating that these two proteins have co-evolved for the regulation of adenosine methylation.

Our work strongly supports the existence of at least two distinct stable complexes that interact weakly to regulate m⁶A biogenesis. This result is consistent with earlier studies by Rottman and colleagues who isolated two protein components using an in vitro methylation assay and HeLa cells nuclear extracts, which are readily dissociable under non-denaturing conditions. Gel filtration and gradient glycerol sedimentation estimated molecular weights of 200 and 875 kDa (Bokar et al. 1997). While biochemical

characterization will be required to address the exact identity of the different complex components, recent biochemical analysis suggests that the 200 kDa complex consists of Mettl3 and Mettl14 (Liu et al. 2014). Although the exact composition of the larger complex is currently unknown, we postulate that it is probably MACOM, consisting of WTAP, VIRMA, HAKAI, RBM15, and ZC3H13. The calculated total molecular weight of these proteins (600 kDa) is lower than the large complex (875 kDa), which suggests the presence of other factors or the inclusion of some subunits in multiple copies. For instance, recombinant WTAP can form aggregates, suggesting the possibility of higher complex organization (Liu et al. 2014). Finally, the existence of two complexes is also supported by our genetic analyses, showing that the knock out of *Mettl3* and *Mettl14* results in viable animals, while loss of function of *fl(2)d*, *vir*, *nito*, and *flacc* are lethal during development. This indicates that the MACOM complex acts beyond m⁶A methylation via METTL3.

The physiological role of ZC3H13 in human cells has been poorly investigated. Recent reports suggest that mutant ZC3H13 facilitates glioblastoma progression and schizophrenia (Oldmeadow et al. 2014; Chow et al. 2017). It is possible that these diseases originate from misregulation of the m⁶A pathway upon ZC3H13 alteration. For instance, the association of m⁶A with cancer progression, in particular with glioblastoma and acute myeloid leukemia, has been recently demonstrated (Yu et al. 2012; Cui et al. 2017; Kwok et al. 2017; Li et al. 2017; Visvanathan et al. 2017; Zhang et al. 2017). Likewise, m⁶A plays an important role in cortical neurogenesis in human forebrain (Yoon et al. 2017), a region of the brain that has been previously associated with schizophrenia (Heimer 2000). Hence, future studies should determine whether the role of ZC3H13 in these diseases is connected to its m⁶A-dependent function.

Materials and Methods

mESC culture and genome editing

Mouse embryonic stem cells (129 × C57Bl/6 genetic background, kindly provided by D. Schübeler of the Friedrich Miescher Institute for Biomedical Research) were cultured on gelatin-coated dishes in mES medium (DMEM, Gibco, 21969-035), supplemented with 15% FBS (Gibco), 1× nonessential amino acids (Gibco), 1 mM sodium pyruvate (Gibco), 2 mM L-glutamine (Gibco), 0.1mM 2-mercaptoethanol (Sigma), 50 mg/ml penicillin, 80 mg/ml streptomycin, MycoZap Prophylactic and LIF conditioned medium) at 37 °C in 5% CO₂. Cultured cells were routinely tested for mycoplasma contamination using the VenorGeM Mycoplasma detection kit (Sigma). For endogenous gene tagging using SpCas9-2A-mCherry (Knuckles et al. 2017), Rosa26:BirA-V5-expressing cells (RosaB) were transfected with 2 μg of SpCas9-sgRNA-2A-mCherry and 500ng of ssODN as donor when integration was desired. Small guide RNAs constructs were generated as described in (Knuckles et al. 2017). The ssODNs were synthesized as Ultramers by Integrated DNA Technologies, and their sequences are listed in Supplementary Table 2. All transfections were carried out using Lipofectamine 3000 reagent (Invitrogen). 24 h post-transfection, mCherry-positive edited cells were sorted on a BD FACSAria III cell sorter (Becton Dickinson). mES cells were then sparsely seeded for clonal expansion, then clones individually picked, split, and screened by PCR for desired mutation or integration. For tagging of *Mettl3* and *Rbm15* clones were subsequently screened by western blotting using anti FLAG (Sigma) or HRP-coupled Streptavidin to confirm expression of endogenously tagged proteins. For *Zc3h13* KO lines, two independent sgRNA constructs were transfected to target sequences flanking exons 9-10 leading to a frame-shift mutation and non-functional truncated protein.

Deletion was confirmed via western blotting using an anti Zc3h13 antibody (Abcam ab70802). Sequences of small guide RNAs are described in Supplementary Table 2.

***Drosophila* stocks and genetics**

Drosophila melanogaster w^{1118} were used as wild-type controls. Other fly stocks used were: Fl(2)d shRNA (HMC03833, BDSC_55674), Nito shRNA (HMS00166) obtained from DRSC, Harvard, Flacc dsRNA (GD35212, KK110253) obtained from VDRC, Vienna. For genetic interaction studies, *Mettl3*^{null} (Hausmann et al. 2016), *Mettl14*^Δ (Lence et al. 2016), *Ythdc1*^{MI02006} (Bloomington), *fl(2)d*² (Bloomington), *vir*^{ts1} (kind gift from Jamilla Horabin), *nito*¹ (Yan and Perrimon 2015) and *flacc* mutant allele *CG7358*^C (Bloomington). To remove *daughterless*, *Df(2L)BSC209* (Bloomington) was used. Driver lines used in this study were *dome*-GAL4 (kind gift from Erika Bach, NYU Langone Medical Center) and *elav*-GAL4 (Bloomington). For the analysis of male to female transformations, flies of selected genotypes were chosen randomly.

***Drosophila* Cell line**

Drosophila S2R+ are embryonic-derived cells obtained from *Drosophila* Genomics Resource Center (DGRC; FlyBase accession FBtc0000150). The presence of Mycoplasma contamination was not tested.

Cloning

The plasmids used for immunohistochemistry and co-immunoprecipitation assays in *Drosophila* S2R⁺ cells were constructed by cloning the corresponding cDNA in the pPAC vector (Lence et al. 2016) with N-terminal Myc tag and the Gateway-based vectors with N-terminal Flag–Myc tag (pPFMW) as well as C-terminal HA tag (pPWH) (obtained from *Drosophila* Genomics Resource Center at Indiana University).

Tandem affinity purification and Mass Spectrometry

One confluent 15cm dish of mESC's per sample was resuspended in 1 ml of ice-cold TAP lysis buffer (NaCl (150 mM-500mM depending on experiment), Tris-HCl (pH 7.5) 20 mM, NP-40 0.5%, EDTA 1 mM, Glycerol 10% and DTT 1 mM supplemented with protease inhibitor cocktail (Roche)) after Trypsin/EDTA (0.25%) dissociation and PBS wash. Samples were shaken at 1,000 rpm at 4°C for 30 min. Lysate was cleared by centrifugation at 4°C at maximum speed on a tabletop centrifuge. Protein concentration of each sample was determined using Bradford assay (Bio-Rad Dye). Equal amounts of lysate (5 mg) from the control sample (parental untagged cells) and the bait-protein sample (gene tagged cells) were normalized adding an appropriate amount of cold TAP lysis buffer to each sample to adjust the final sample concentration to be ~5 mg/mL. Equilibrated FLAG M2 Dynabeads (Sigma, 10 μ l of packed bead slurry per 5 mg protein / sample) previously washed twice with 1 ml of cold TAP lysis buffer, were added to each 5mg/mL lysate. Tubes containing beads and lysates were incubated with end-over-end rotating at 4°C overnight.

Dynabeads were washed the next day in TAP buffer (4x10min), followed by 3x15min elution of bound proteins with 3xFLAG peptide (final concentration of 0.3 mg.ml⁻¹ in

TAP buffer, Sigma). Next, elutions were pooled and added to the TAP washed Streptavidin Dynabeads (ThermoFisher), and incubated overnight, rotating at 4°C. Streptavidin Dynabeads were washed the next day with TAP buffer (4x10min), followed by a wash with TAP buffer without NP40. The enriched proteins were digested directly on the Dynabeads with 0.1 mg.ml⁻¹ trypsin in Digestion buffer (50mM Tris pH 8.0, 1mM CaCl₂, 1mM TCEP).

The generated peptides were acidified with TFA to a final concentration of 0.8% and analyzed by capillary liquid chromatography tandem mass spectrometry with an EASY-nLC 1000 using the two-column set-up (Thermo Scientific). The peptides were loaded with 0.1% formic acid, 2% acetonitrile in H₂O onto a peptide trap (Acclaim PepMap 100, 75um x 2cm, C18, 3um, 100Å) at a constant pressure of 800 bar. Peptides were separated, at a flow rate of 150 nl/min with a linear gradient of 2–6% buffer B in buffer A in 3 minutes followed by an linear increase from 6 to 22% in 40 minutes, 22-28% in 9 min, 28-36% in 8min, 36-80% in 1 min, and the column was finally washed for 14 min at 80% B (Buffer A: 0.1% formic acid, buffer B: 0.1% formic acid in acetonitrile) on a 50um x 15cm ES801 C18, 2um, 100Å column (Thermo Scientific) mounted on a DPV ion source (New Objective) connected to an Orbitrap Fusion mass spectrometer (Thermo Scientific). The data were acquired using 120000 resolution for the peptide measurements in the Orbitrap and a top T (3s) method with HCD fragmentation for each precursor and fragment measurement in the ion trap according to the recommendation of the manufacturer (Thermo Scientific).

Protein identification and relative quantification of the proteins was done with MaxQuant version 1.5.3.8 using Andromeda as search engine (Cox et al. 2011) and label free quantification (LFQ (Cox et al. 2014)) as described in (Hubner et al. 2010). The mouse subset of the UniProt version 2015_01 combined with the contaminant DB from

MaxQuant was searched and the protein and peptide FDR were set to 0.01. All MaxQuant parameters can be found in the uploaded parameterfile: mqpar.xml.

Statistical analysis was done in Perseus (version 1.5.2.6) (Cox et al. 2011; Cox et al. 2014; Tyanova et al. 2016). Results were filtered to remove reverse hits, contaminants and peptides found in only one sample. Missing values were imputed and potential interactors were determined using t-test and visualized by a volcano plot. Significance lines corresponding to a given FDR have been determined by a permutation-based method (Tusher et al. 2001). Threshold values (FDR) were selected between 0.005 and 0.05 and SO (curve bend) between 0.2 and 2 and are shown in the corresponding figures. Results were exported from Perseus and visualized using statistical computing language R.

iBAQ Analysis

Intensity based absolute quantification (iBAQ) was performed as described in (Schwanhausser et al. 2011) to evaluate protein abundances in MAC and MACOM complexes in Mettl3 TAP-LC-MS experiments.

m⁶A RNA immunoprecipitation

Total RNA from mESCs was isolated using Absolutely RNA Microprep Kit (Stratagene), followed by mRNA selection using double Oligo d(T)23 (NEB) purification. 5 µg mRNA cells was incubated with 4 µg of anti-m⁶A antibody (Synaptic Systems; polyclonal Rabbit - Cat. No. 202 003) in m⁶A-IP buffer (150 mM NaCl, 10 mM Tris-HCl pH 7.4, 0.1% NP-40) supplemented with 5 U /mL of Murine RNase inhibitor (NEB) for 2 h at 4°C. 10 µL of protein G magnetic beads (Invitrogen) were added to all m⁶A-IP samples for 2 h at 4°C. On bead digestion with RNase T1 (Thermo

Fisher) at final concentration 0.1 U/mL was performed for 15 min at RT. Beads with captured RNA fragments were then immediately washed 2 times with 500 μ L of ice-cold m⁶A-IP buffer, 2 times with RT m⁶A-IP buffer and further eluted with 100 μ L of elution buffer (20 mM DTT, 150 mM NaCl, 50 mM Tris-HCl pH 7.4, 1 mM EDTA, 0.1% SDS, 5 U/mL Proteinase K) at 42°C for 5 min. Elution step was repeated 4 times and 600 μ L of acidic phenol/chloroform pH 4.5 (Ambion) was added to 400 μ L of the combined eluate per sample in order to extract captured RNA fragments. Samples were mixed and transferred to Phase Lock Gel Heavy tubes (5Prime) and centrifuged for 5 min at 12000x g. Aqueous phase was precipitated O/N, -80°C. On the following day, samples were centrifuged, washed twice with 80% EtOH and re-suspended in 15 μ L of RNase-free H₂O (Ambion). Recovered RNA was analyzed on RNA Pico Chip (Agilent) and concentrations were determined with RNA HS Qubit reagents. Since no RNA was recovered in the m⁶A-IP no-antibody control samples, libraries were prepared with 30 ng of two independent m⁶A-IPs performed on RNA from WT, *Mettl3* and *Zc3h13* KO cells. For every condition, input material (200ng mRNA) was also sequenced. Both m⁶A-IPs and inputs were sequenced using the NEB-Next RNA Directional Library Preparation Kit.

m⁶A-RNA immunoprecipitation sequencing analysis

MACS2 was used to call peaks of m⁶A enrichment for wildtype and H4 IP vs input samples, using the default parameters. Peaks were assigned to overlapping gene bodies within 500 bp. The intersection of the resulting gene lists (3285 genes) was taken as the set of m⁶A target genes.

BigWig files for each sample were created using the qExportWig function from the QuasR package in R (Gaidatzis et al. 2015). Read counts were binned in 50 bp windows, and counts for each sample were scaled to the mean aligned library size of all samples. The deepTools suite was used for metagene analysis (Ramirez et al. 2016). The bigwigCompare function was used to calculate the log₂ ratio between each wildtype or ZC3H13-KO sample and the Mettl3-KO samples. m⁶A target CDS regions were scaled to 5 kb, and m⁶A enrichment vs. Mettl3-KO was calculated in 50-bp bins across scaled target regions as well as 2 kb up- and downstream using the computeMatrix command.

NanoBiT protein complementation assay

Fusion construct of mouse Rbm15 and Wtap to NanoBiT subunits were generated as follows: Full length Rbm15 and Wtap coding sequences were amplified with oligonucleotides indicated in Supplementary Table 2 from poly-A selected mRNA using NEBNext High-Fidelity 2X PCR Master Mix (New England BioLabs). Overhangs with homology to destination vectors (pBiT1.1-C, pBiT2.1-C, pBiT1.1-N, pBiTN.1-C; Promega) were included in oligonucleotide sequences. Gel purified PCR products were cloned into EcoRI sites using NEBuilder HiFi DNA assembly kit (New England BioLabs) following manufacturers recommendations. The optimal combination of N or C-termini tagged fusions to small (Sm) or large (Lg) subunits, were determined through transfection of 20,000 cells/well WT mESC's cells with Lipofectamine 3000 reagent (Invitrogen) seeded in 96-well tissue culture plates (Corning Cat. #3917). Measurements were performed using the Nano-Glo Live cells Assay system (Promega) and measured in a microplate luminometer (Berthold LB960). The Rbm15/Wtap fusion combination yielding the highest luciferase activity was then transfected into distinct mESC genetic

backgrounds and expression level of fusion construct quantified via RT-qPCR using oligonucleotides described in Supplementary Table 2.

***Drosophila* staging**

Staging experiment was performed as described previously (Lence et al. 2016) using *Drosophila melanogaster* *w¹¹¹⁸* flies. A total of three independent samples were collected for each *Drosophila* stage as well as for heads and ovaries. Samples from the staging experiment were used for RNA extraction to analyse m⁶A abundance in mRNA and expression levels of different transcripts during *Drosophila* development.

RNA isolation and mRNA purification

Total RNA from S2R+ cells was isolated using Trizol reagent (Invitrogen) and DNA was removed with DNase-I treatment (NEB). Fly heads from 3-5 day old flies were separated and homogenized in Trizol prior to RNA isolation. mRNA was isolated by two rounds of purification with Dynabeads Oligo d(T)25 (NEB).

RT-PCR

cDNA was prepared using M-MLV Reverse Transcriptase (Promega). Transcript levels were quantified using Power SYBR Green PCR Master Mix (Invitrogen) and oligonucleotides indicated in Supplementary Table 2. RT-PCR was performed using the oligonucleotides described in Supplementary Table 2 to analyse *Sxl* splicing.

RNA *in situ* hybridization

For *in situ* hybridization *Drosophila melanogaster* *w¹¹¹⁸* flies were kept at 25 °C in conical flasks with apple juice agar plates and embryos were collected every 24 h. Embryos were transferred in a sieve and dechorionated for 2 min in 50% sodium hypochloride. After 5 min wash in water, embryos were permeabilized with PBST (0.1% Tween X-100 in PBS) for 5 min. Embryos were transferred in 1:1 mixture of heptane (Sigma) and 8% formaldehyde (Sigma) and fixed for 20 min with constant shaking at room temperature. After fixation the lower organic phase was removed and 1 volume of MeOH was added to the aqueous phase containing fixed embryos. Following 5 min of extensive shaking all liquid was removed and embryos were washed 3 times with 100% MeOH. At this point embryos were stored at -20 °C or used for further analysis. For *in situ* hybridization MeOH was gradually replaced with PBST with 10 min washes and with three final washes in PBST. Embryos were further washed for 10 min at room temperature with 50% HB4 solution (50% formamide, 5× SSC, 50 µg/ml heparin, 0,1% Tween, 5 mg/ml torula yeast extract) diluted in PBST. Blocking was performed with HB4 solution, first for 1 h at room temperature and next for 1 h at 65 °C. *In situ* probes were prepared with DIG RNA labelling Kit (Roche) following the manufacturer's protocol. Two microlitres of the probe were diluted in 200 µl of HB4 solution, heated up to 65 °C to denature the RNA secondary structure and added to blocked embryos for further overnight incubation at 65 °C. The next day, embryos were washed 2 times for 30 min at 65 °C with formamide solution (50% formamide, 1× SSC in PBST) and further 3 times for 20 min at room temperature with PBST. Embryos were then incubated with anti-DIG primary antibody (Roche) diluted in PBST (1:2,000) for 2 h at room temperature and later washed 5 times for 30 min with PBST. In order to develop the

staining, embryos were rinsed with AP buffer (100 mM Tris pH 9.5, 50 mM MgCl₂, 100 mM NaCl, 0.1% Tween) and incubated with NBT/BCIP solution in AP buffer (1:100 dilution) until the intense staining was observed. Reaction was stopped with several 15 min PBST washes. Prior to mounting, embryos were incubated in 20% glycerol and later visualized on Leica M205-FA stereomicroscope.

RNA immunoprecipitation (RIP)

S2R⁺ cells were transfected with Myc-tagged constructs using Effectene reagent. 72 h post transfection cells were washed with ice cold PBS and collected by 5 min centrifugation at 1000x g. The cell pellet was lysed in 1 ml of lysis buffer (50 mM Tris-HCl, pH 7.4, 150 mM NaCl, 0.05% NP-40) supplemented with protease inhibitors, rotated head-over-tail for 30 min at 4 °C and centrifuged at 18,000x g for 10 min at 4 °C to remove the remaining cell debris. Protein concentrations were determined using Bradford reagent (BioRad). For RNA immunoprecipitation, 2 mg of proteins were incubated with 2 µg of anti-Myc antibody coupled to protein-G magnetic beads (Invitrogen) in lysis buffer and rotated head-over-tail for 4h at 4 °C. The beads were washed 3 times for 5 min with washing buffer. One fourth of immunoprecipitated protein – RNA complexes were eluted by incubation in 1× NuPAGE LDS buffer (Thermo Fisher) at 70 °C for 10 min for protein analysis. RNA from the remaining protein-RNA complexes was further isolated using Trizol reagent.

Immunostaining

For staining of *Drosophila* S2R⁺ cells, cells were transferred to the poly-lysine pre-treated 8-well chambers (Ibidi) at the density of 2×10^5 cells/well. After 30 min, cells were washed with 1× DPBS (Gibco), fixed with 4% formaldehyde for 10 min and permeabilized with PBST (0.2% Triton X-100 in PBS) for 15 min. Cells were incubated with mouse anti-Myc (1:2000; #9E10, Enzo) in PBST supplemented with 10% of donkey serum at 4 °C, overnight. Cells were washed 3× for 15 min in PBST and then incubated with secondary antibody and 1× DAPI solution in PBST supplemented with 10% of donkey serum for 2 h at 4 °C. After three 15 min washes in PBST, cells were imaged with Leica SP5 confocal microscope using ×63 oil immersion objective.

Western blotting

Proteins were extracted for 30 min on ice, the lysates were centrifuged at $16,000 \times g$ for 5 min at 4°C , and protein concentration in the supernatant was determined using the Bio-Rad protein assay. Protein samples were separated on NuPAGE-Novex Bis-Tris 4-12% gradient gels (Invitrogen) in MOPS buffer at 200V for 40 min. Semi-dry transfer to nitrocellulose membrane (Whatman) was performed at 15 V for 40 min. Membranes were blocked for 30 min 2% non-fat dry milk in TBS-0.05% Tween 20 (TBST), and incubated with primary antibodies at 4°C overnight (Mettl3 (Protein Tech 15073), Rbm15 (Abcam ab70549), Zc3h13 (Abcam ab70802), Hakai (Cbl11 ARP39622, Aviva systems biology), Wtap (Protein Tech 60188) and Tubulin (Abcam clone YL1/2). Signal was detected with corresponding HRP-conjugated secondary antibodies and Immobilon Western Chemiluminiscent HRP Substrate (Millipore).

Cell culture, RNA interference and transfection

Drosophila S2R⁺ cells were grown in Schneider's medium (Gibco) supplemented with 10% FBS (Sigma) and 1% penicillin–streptomycin (Sigma). For RNA interference (RNAi) experiments, PCR templates were prepared using oligonucleotides indicated in Supplementary Table 2. dsRNA were prepared using T7 megascript Kit (NEB). dsRNA against bacterial beta-galactosidase gene (lacZ) was used as a control for all RNA interference (RNAi) experiments. S2R⁺ cells were seeded at the density of 10^6 cells/ml in serum-free medium and 7.5 μg of dsRNA was added to 10^6 cells. After 6 h of cell starvation, serum supplemented medium was added to the cells. dsRNA treatment was repeated after 48 and 96 h and cells were collected 24 h after the last treatment.

Effectene (Qiagen) was used to transfect vector constructs in all overexpression experiments following the manufacturer's protocol.

Co-immunoprecipitation assay and western blot analysis

For the co-immunoprecipitation assay, different combinations of vectors with indicated tags were co-transfected in S2R+ cells. Forty-eight hours after transfection cells were collected, washed with DPBS and pelleted by 10 min centrifugation at 400g. The cell pellet was lysed in 1 ml of lysis buffer (50 mM Tris-HCl, pH 7.4, 150 mM NaCl, 0.05% NP-40) supplemented with protease inhibitors and rotated head-over-tail for 30 min at 4 °C. Nuclei were collected by 10 min centrifugation at 1,000g at 4 °C re-suspended in 300 µl of lysis buffer and sonicated with 5 cycles of 30 s ON, 30 s OFF low power setting. Cytoplasmic and nuclear fractions were joined and centrifuged at 18,000x g for 10 min at 4 °C to remove the remaining cell debris. Protein concentrations were determined using Bradford reagent (BioRad). For immunoprecipitation, 2 mg of proteins were incubated with 2 µg of anti-Myc antibody coupled to protein-G magnetic beads (Invitrogen) in lysis buffer and rotated head-over-tail overnight at 4 °C. The beads were washed 3 times for 15 min with lysis buffer and immunoprecipitated proteins were eluted by incubation in 1× NuPAGE LDS buffer (Thermo Fisher) at 70 °C for 10 min. Eluted immunoprecipitated proteins were removed from the beads and DTT was added to 10% final volume. Immunoprecipitated proteins and input samples were analysed by western blot after incubation at 70 °C for additional 10 min.

For western blot analysis, proteins were separated on 7% SDS-PAGE gel and transferred on Nitrocellulose membrane (BioRad). After blocking with 5% milk in PBST (0.05% Tween in PBS) for 1 h at room temperature, the membrane was incubated with primary

antibody in blocking solution overnight at 4 °C. Primary antibodies used were: mouse anti-Myc 1:2,000 (#9E10, Enzo); mouse anti-HA 1:1,000 (#16B12, COVANCE); mouse anti-Tubulin 1:2,000 (#903401, Biolegend); mouse anti-Fl(2)d 1:500 (#9G2, DSHB); rabbit anti-Mettl14 and guinea pig anti-Mettl3 1:500 (Lence et al. 2016). The membrane was washed 3 times in PBST for 15 min and incubated 1 h at room temperature with secondary antibody in blocking solution. Protein bands were detected using SuperSignal West Pico Chemiluminescent Substrate (Thermo Scientific).

SILAC experiment and LC–MS/MS analysis

For SILAC experiments, S2R+ cells were grown in Schneider medium (Dundee Cell) supplemented with either heavy (Arg8, Lys8) (Cambridge Isotope Laboratories) or light amino acids (Arg0, Lys0) (Sigma). For the forward experiment, Myc–Nito was transfected in heavy-labelled cells and Myc-alone in light-labelled cells. The reverse experiment was performed vice versa. The co-immunoprecipitation experiment was done as described earlier. Before elution, beads of the heavy and light lysates were combined in 1:1 ratio and eluted with 1× NuPAGE LDS buffer that was subject to MS analysis as described previously (Bluhm et al. 2016). Raw files were processed with MaxQuant (version 1.5.2.8) and searched against the Uniprot database of annotated *Drosophila* proteins (*Drosophila melanogaster*: 41,850 entries, downloaded 8 January 2015).

LC–MS/MS analysis of m⁶A levels

Three-hundred nanograms of purified mRNA was digested using 0.3 U Nuclease P1 from *Penicillium citrinum* (Sigma-Aldrich, Steinheim, Germany) and 0.1 U Snake venom

phosphodiesterase from *Crotalus adamanteus* (Worthington, Lakewood, USA). RNA and enzymes were incubated in 5 mM ammonium acetate at pH 5.3 for 2 h at 37 °C. Remaining phosphates were removed by 1 U FastAP (Thermo Scientific, St Leon-Roth, Germany) in a 1 h incubation at 37 °C in 10 mM ammonium acetate at pH 8. The resulting nucleoside mix was then spiked with ¹³C stable isotope labelled nucleoside mix from *Escherichia coli* RNA as an internal standard (SIL-IS) to a final concentration of 6 ng/μl for the sample RNA and 2 ng/μl for the SIL-IS. For analysis, 10 μl of the before mentioned mixture were injected into the LC–MS/MS machine. Generation of technical triplicates was obligatory. Mouse mRNA samples were analysed in biological duplicates and fly samples in triplicates. LC separation was performed on an Agilent 1200 series instrument, using 5 mM ammonium acetate buffer as solvent A and acetonitrile as buffer B. Each run started with 100% buffer A, which was decreased to 92% within 10 min. Solvent A was further reduced to 60% within another 10 min. Until minute 23 of the run, solvent A was increased to 100% again and kept at 100% for 7 min to re-equilibrate the column (Synergi Fusion, 4 μM particle size, 80 Å pore size, 250 × 2.0 mm, Phenomenex, Aschaffenburg, Germany). The ultraviolet signal at 254 nm was recorded via a DAD detector to monitor the main nucleosides.

MS/MS was then conducted on the coupled Agilent 6460 Triple Quadrupole (QQQ) mass spectrometer equipped with an Agilent JetStream ESI source which was set to the following parameters: gas temperature, 350 °C; gas flow, 8 l/min; nebulizer pressure, 50 psi; sheath gas temperature, 350 °C; sheath gas flow, 12 l/min; and capillary voltage, 3,000 V. To analyse the mass transitions of the unlabelled m⁶A and all ¹³C m⁶A simultaneously, we used the dynamic multiple reaction monitoring mode. The quantification was conducted as described previously (Kellner et al. 2014)

RNA-seq and Computational analysis

Illumina TruSeq Sequencing Kit (Illumina) was used. The RNA libraries were sequenced on a NextSeq500 with a read length of 85 bp. The data was mapped against Ensembl release 90 of *Drosophila Melanogaster* using STAR (v2.5.1b). Counts per gene were derived using featureCounts (v.1.5.1). Differential expression analysis was performed using DESeq2 (v. 1.16.1) and filtered for an FDR < 1%. Differentially splicing analysis was performed using rMATS (v 3.2.5) and filtered for an FDR < 10%. Sequencing depth normalised coverage tracks were generated using bedtools (v.2.25.0), samtools (v.1.3.1) and kentutils (v.302). Heatmap of the foldchange (log₂) of commonly misregulated genes was clustered according to rows and columns. The color gradient was adjusted to display the 1% lowest/highest values within the most extreme color (lowest values as the darkest blue, highest values as the darkest red). Splice events for different knockdown conditions are represented by pie charts. “Control” depicts the detected splice events on average in all the comparisons Control vs. knockdown. The pie charts for the individual knockdowns depict the amount of significantly different splicing events with a FDR value below 10%. The GO term analysis was performed using the package ClusterProfiler. The GO -terms were semantic similarity reduced using the “simplify” function of the package. The tested genes in all the conditions were used as a background gene set. Default parameters were used for the analysis (Yu et al. 2012). m⁶A gene annotation was retrieved from mCLIP paper (Kan et al. 2017b). m⁶A containing gene names were translated to used annotation and filtered for tested genes in the differential expression analysis (in any condition). These genes were overlapped with the genes commonly differentially regulated in the knockdowns (either commonly up, commonly down or mis-regulated in all conditions). Similarly, the m⁶A containing genes were

overlapped with the genes commonly mis-spliced in all conditions. The significance of the overlap was tested using a hypergeometric test.

Phylogenetic analysis

The phylogenetic tree was constructed with ClustalX from multiple sequence alignments generated with MUSCLE of the *Drosophila* sequence with orthologs from human and other representative species.

Data availability statement

The data that support the findings of this study have been deposited in the NCBI Gene Expression Omnibus (GEO) under accession GSE106614. All other relevant data are available from the corresponding author.

Acknowledgments

We would like to thank the Bloomington *Drosophila* Stock Center and the Vienna *Drosophila* Resource Center for fly reagents; the *Drosophila* Genomics Resource Center at Indiana University for plasmids; members of the Bühler and Roignant labs for helpful discussion; Vytautas Iesmantavicius from the Protein Analysis Facility at FMI for help with MS data analysis, the Genomics and Bioinformatics IMB core facilities for great support. Support by IMB Proteomics core facility is gratefully acknowledged (instrument is funded by DFG INST 247/766-1 FUGG). In particular, we wish to thank Anja Freiwald from IMB Proteomics core facility for sample preparation and Dr. Mario Dejung from Proteomics core facility for data processing and generating the scatter plot. Research in the laboratory of J.-Y.R. is supported by the Deutsche Forschungsgemeinschaft RO 4681/5-1 and the Epitran COST action (CA16120). Work performed in M.B.'s laboratory was supported by the Novartis Research Foundation and the Swiss Science Foundation NCCR RNA & Disease (grant no. 141735). Work performed in M.S.'s laboratory was supported by the BBSRC. The project was also supported by the DFG SPP1784 Grant to M.H.

Author contributions

Conceptualization, P.K, T.L., M.B. and J.Y.R.; Methodology, P.K., T.L., I.U.H, D.J., I.M., T.H., R.V., D.H., M.B., M.H., M.S., M.B. and J.Y.R.; Computational analysis of RNA-Seq, N. K.; Computational analysis of meRIP-Seq, S.H.C.; Phylogenetic analysis, M.A.A.N. Writing – Original Draft, P.K. and T.L.; Writing –Review & Editing, all authors; Supervision, M.B and J.Y.R.

References

- Agarwala SD, Blitzblau HG, Hochwagen A, Fink GR. 2012. RNA methylation by the MIS complex regulates a cell fate decision in yeast. *PLoS genetics* **8**: e1002732.
- Ashburner M, Ball CA, Blake JA, Botstein D, Butler H, Cherry JM, Davis AP, Dolinski K, Dwight SS, Eppig JT et al. 2000. Gene ontology: tool for the unification of biology. The Gene Ontology Consortium. *Nature genetics* **25**: 25-29.
- Bluhm A, Casas-Vila N, Scheibe M, Butter F. 2016. Reader interactome of epigenetic histone marks in birds. *Proteomics* **16**: 427-436.
- Bokar JA, Shambaugh ME, Polayes D, Matera AG, Rottman FM. 1997. Purification and cDNA cloning of the AdoMet-binding subunit of the human mRNA (N6-adenosine)-methyltransferase. *Rna* **3**: 1233-1247.
- Chow RD, Guzman CD, Wang G, Schmidt F, Youngblood MW, Ye L, Errami Y, Dong MB, Martinez MA, Zhang S et al. 2017. AAV-mediated direct in vivo CRISPR screen identifies functional suppressors in glioblastoma. *Nature neuroscience*.
- Cox J, Hein MY, Lubner CA, Paron I, Nagaraj N, Mann M. 2014. Accurate proteome-wide label-free quantification by delayed normalization and maximal peptide ratio extraction, termed MaxLFQ. *Molecular & cellular proteomics : MCP* **13**: 2513-2526.
- Cox J, Neuhauser N, Michalski A, Scheltema RA, Olsen JV, Mann M. 2011. Andromeda: a peptide search engine integrated into the MaxQuant environment. *Journal of proteome research* **10**: 1794-1805.
- Cui Q, Shi H, Ye P, Li L, Qu Q, Sun G, Sun G, Lu Z, Huang Y, Yang CG et al. 2017. m6A RNA Methylation Regulates the Self-Renewal and Tumorigenesis of Glioblastoma Stem Cells. *Cell reports* **18**: 2622-2634.
- Dezi V, Ivanov C, Haussmann IU, Soller M. 2016. Nucleotide modifications in messenger RNA and their role in development and disease. *Biochemical Society transactions* **44**: 1385-1393.
- Dixon AS, Schwinn MK, Hall MP, Zimmerman K, Otto P, Lubben TH, Butler BL, Binkowski BF, Machleidt T, Kirkland TA et al. 2016. NanoLuc Complementation Reporter Optimized for Accurate Measurement of Protein Interactions in Cells. *ACS chemical biology* **11**: 400-408.
- Dominissini D, Moshitch-Moshkovitz S, Schwartz S, Salmon-Divon M, Ungar L, Osenberg S, Cesarkas K, Jacob-Hirsch J, Amariglio N, Kupiec M et al. 2012. Topology of the human and mouse m6A RNA methylomes revealed by m6A-seq. *Nature* **485**: 201-206.
- Flemr M, Buhler M. 2015. Single-Step Generation of Conditional Knockout Mouse Embryonic Stem Cells. *Cell reports* **12**: 709-716.
- Gaidatzis D, Lerch A, Hahne F, Stadler MB. 2015. QuasR: quantification and annotation of short reads in R. *Bioinformatics* **31**: 1130-1132.
- Haussmann IU, Bodi Z, Sanchez-Moran E, Mongan NP, Archer N, Fray RG, Soller M. 2016. m6A potentiates Sxl alternative pre-mRNA splicing for robust *Drosophila* sex determination. *Nature* **540**: 301-304.

- Heimer L. 2000. Basal forebrain in the context of schizophrenia. *Brain research Brain research reviews* **31**: 205-235.
- Hilfiker A, Amrein H, Dubendorfer A, Schneiter R, Nothiger R. 1995. The gene *virilizer* is required for female-specific splicing controlled by *Sxl*, the master gene for sexual development in *Drosophila*. *Development* **121**: 4017-4026.
- Horiuchi K, Kawamura T, Iwanari H, Ohashi R, Naito M, Kodama T, Hamakubo T. 2013. Identification of Wilms' tumor 1-associating protein complex and its role in alternative splicing and the cell cycle. *The Journal of biological chemistry* **288**: 33292-33302.
- Hubner NC, Bird AW, Cox J, Splettstoesser B, Bandilla P, Poser I, Hyman A, Mann M. 2010. Quantitative proteomics combined with BAC TransgeneOmics reveals in vivo protein interactions. *The Journal of cell biology* **189**: 739-754.
- Kan L, Grozhik AV, Vedanayagam J, Patil DP, Pang N, Lim KS, Huang YC, Joseph B, Lin CJ, Despic V et al. 2017a. The m6A pathway facilitates sex determination in *Drosophila*. *Nature communications* **8**: 15737.
- . 2017b. The m(6)A pathway facilitates sex determination in *Drosophila*. *Nature communications* **8**: 15737.
- Kellner S, Ochel A, Thuring K, Spenkuch F, Neumann J, Sharma S, Entian KD, Schneider D, Helm M. 2014. Absolute and relative quantification of RNA modifications via biosynthetic isotopomers. *Nucleic acids research* **42**: e142.
- Knuckles P, Carl SH, Musheev M, Niehrs C, Wenger A, Buhler M. 2017. RNA fate determination through cotranscriptional adenosine methylation and microprocessor binding. *Nature structural & molecular biology* **24**: 561-569.
- Kwok CT, Marshall AD, Rasko JE, Wong JJ. 2017. Genetic alterations of m6A regulators predict poorer survival in acute myeloid leukemia. *Journal of hematology & oncology* **10**: 39.
- Lence T, Akhtar J, Bayer M, Schmid K, Spindler L, Ho CH, Kreim N, Andrade-Navarro MA, Poeck B, Helm M et al. 2016. m6A modulates neuronal functions and sex determination in *Drosophila*. *Nature* **540**: 242-247.
- Lence T, Soller M, Roignant JY. 2017. A fly view on the roles and mechanisms of the m6A mRNA modification and its players. *RNA biology*: 1-9.
- Li Z, Weng H, Su R, Weng X, Zuo Z, Li C, Huang H, Nachtergaele S, Dong L, Hu C et al. 2017. FTO Plays an Oncogenic Role in Acute Myeloid Leukemia as a N6-Methyladenosine RNA Demethylase. *Cancer cell* **31**: 127-141.
- Liu J, Yue Y, Han D, Wang X, Fu Y, Zhang L, Jia G, Yu M, Lu Z, Deng X et al. 2014. A METTL3-METTL14 complex mediates mammalian nuclear RNA N6-adenosine methylation. *Nature chemical biology* **10**: 93-95.
- Meyer KD, Saletore Y, Zumbo P, Elemento O, Mason CE, Jaffrey SR. 2012. Comprehensive analysis of mRNA methylation reveals enrichment in 3' UTRs and near stop codons. *Cell* **149**: 1635-1646.
- Oldmeadow C, Mossman D, Evans TJ, Holliday EG, Tooney PA, Cairns MJ, Wu J, Carr V, Attia JR, Scott RJ. 2014. Combined analysis of exon splicing and genome wide polymorphism data predict schizophrenia risk loci. *Journal of psychiatric research* **52**: 44-49.

- Patil DP, Chen CK, Pickering BF, Chow A, Jackson C, Guttman M, Jaffrey SR. 2016a. m6A RNA methylation promotes XIST-mediated transcriptional repression. *Nature* **537**: 369-373.
- . 2016b. m(6)A RNA methylation promotes XIST-mediated transcriptional repression. *Nature* **537**: 369-373.
- Ping XL, Sun BF, Wang L, Xiao W, Yang X, Wang WJ, Adhikari S, Shi Y, Lv Y, Chen YS et al. 2014. Mammalian WTAP is a regulatory subunit of the RNA N6-methyladenosine methyltransferase. *Cell research* **24**: 177-189.
- Ramirez F, Ryan DP, Gruning B, Bhardwaj V, Kilpert F, Richter AS, Heyne S, Dundar F, Manke T. 2016. deepTools2: a next generation web server for deep-sequencing data analysis. *Nucleic acids research* **44**: W160-165.
- Roignant JY, Soller M. 2017. m6A in mRNA: An Ancient Mechanism for Fine-Tuning Gene Expression. *Trends in genetics : TIG* **33**: 380-390.
- Ruzicka K, Zhang M, Campilho A, Bodi Z, Kashif M, Saleh M, Eeckhout D, El-Showk S, Li H, Zhong S et al. 2017. Identification of factors required for m6A mRNA methylation in Arabidopsis reveals a role for the conserved E3 ubiquitin ligase HAKAI. *The New phytologist* **215**: 157-172.
- Schwanhauser B, Busse D, Li N, Dittmar G, Schuchhardt J, Wolf J, Chen W, Selbach M. 2011. Global quantification of mammalian gene expression control. *Nature* **473**: 337-342.
- Schwartz S, Mumbach MR, Jovanovic M, Wang T, Maciag K, Bushkin GG, Mertins P, Ter-Ovanesyan D, Habib N, Cacchiarelli D et al. 2014. Perturbation of m6A writers reveals two distinct classes of mRNA methylation at internal and 5' sites. *Cell reports* **8**: 284-296.
- Sledz P, Jinek M. 2016. Structural insights into the molecular mechanism of the m(6)A writer complex. *eLife* **5**.
- Tusher VG, Tibshirani R, Chu G. 2001. Significance analysis of microarrays applied to the ionizing radiation response. *Proceedings of the National Academy of Sciences of the United States of America* **98**: 5116-5121.
- Tyanova S, Temu T, Sinitcyn P, Carlson A, Hein MY, Geiger T, Mann M, Cox J. 2016. The Perseus computational platform for comprehensive analysis of (prote)omics data. *Nature methods* **13**: 731-740.
- Visvanathan A, Patil V, Arora A, Hegde AS, Arivazhagan A, Santosh V, Somasundaram K. 2017. Essential role of METTL3-mediated m6A modification in glioma stem-like cells maintenance and radioresistance. *Oncogene*.
- Wan C, Borgeson B, Phanse S, Tu F, Drew K, Clark G, Xiong X, Kagan O, Kwan J, Bezginov A et al. 2015. Panorama of ancient metazoan macromolecular complexes. *Nature* **525**: 339-344.
- Wang P, Doxtader KA, Nam Y. 2016a. Structural Basis for Cooperative Function of Mettl3 and Mettl14 Methyltransferases. *Molecular cell* **63**: 306-317.
- Wang X, Feng J, Xue Y, Guan Z, Zhang D, Liu Z, Gong Z, Wang Q, Huang J, Tang C et al. 2016b. Structural basis of N(6)-adenosine methylation by the METTL3-METTL14 complex. *Nature* **534**: 575-578.
- Wang Y, Li Y, Toth JI, Petroski MD, Zhang Z, Zhao JC. 2014. N6-methyladenosine modification destabilizes developmental regulators in embryonic stem cells. *Nature cell biology* **16**: 191-198.

- Yan D, Perrimon N. 2015. *spenito* is required for sex determination in *Drosophila melanogaster*. *Proceedings of the National Academy of Sciences of the United States of America* **112**: 11606-11611.
- Yoon KJ, Ringeling FR, Vissers C, Jacob F, Pokrass M, Jimenez-Cyrus D, Su Y, Kim NS, Zhu Y, Zheng L et al. 2017. Temporal Control of Mammalian Cortical Neurogenesis by m6A Methylation. *Cell*.
- Yu G, Wang LG, Han Y, He QY. 2012. clusterProfiler: an R package for comparing biological themes among gene clusters. *OmicS : a journal of integrative biology* **16**: 284-287.
- Zhang S, Zhao BS, Zhou A, Lin K, Zheng S, Lu Z, Chen Y, Sulman EP, Xie K, Bogler O et al. 2017. m6A Demethylase ALKBH5 Maintains Tumorigenicity of Glioblastoma Stem-like Cells by Sustaining FOXM1 Expression and Cell Proliferation Program. *Cancer cell* **31**: 591-606 e596.
- Zhong S, Li H, Bodi Z, Button J, Vespa L, Herzog M, Fray RG. 2008. MTA is an Arabidopsis messenger RNA adenosine methylase and interacts with a homolog of a sex-specific splicing factor. *The Plant cell* **20**: 1278-1288.

Figure legends**Figure 1. Zc3h13/Flacc interacts with the m⁶A machinery**

(A) TAP-LC-MS/MS of endogenously FLAG-Avi tagged Rbm15 mESC's Parental cells were used as background control and proteins were purified in the presence of 350mM NaCl. Highlighted in the volcano plot are enriched proteins that were members of the WTAP complex (red) as well as Zc3h13 (green). (B) Heatmap comparing relative LFQ intensities of selected Mettl3 bound proteins across increasing NaCl concentrations. Statistical analysis was done with Perseus (see methods for details). Mass spectrometry raw data is deposited in ProteomeXchange. (C and D) SILAC-coupled mass spectrometry analysis using Nito-Myc as bait. Scatterplot of normalized forward versus inverted reverse experiments plotted on a log₂ scale. The threshold was set to a 1.5-fold enrichment (red dashed line). Proteins in the upper right quadrant are enriched in both replicates. GO-term analysis (Ashburner et al. 2000) for enriched proteins is shown in (D). (E) Co-immunoprecipitation experiments were carried out with lysates prepared from S2R+ cells, transfected with FlagMyc-Flacc and HA-Nito. In control lanes, S2R+ cells were transfected with FlagMyc alone and identical HA-containing protein. Extracts were immunoprecipitated with Myc antibody and immunoblotted using Flag and HA antibodies. 2% of input was loaded. The same experiment was repeated in the presence of RNaseT1. Nito and Flacc interact with each other in an RNA independent manner. (F) Table representing orthologous proteins of MAC and MACOM complexes in mouse and fly.

Figure 2. Flacc/Zc3h13 regulates the m⁶A pathway

(A) LC-MS/MS quantification of m⁶A levels in mRNA extracts from WT mESC's, *Mettl3* KO, *Mettl3* KO plasmid-rescue, and *Zc3h13* KO cells. Mean of two biological

replicates and three independent measurements is shown; errors bars indicate standard deviation (s.d.). *, $P < 0.01$ and n.s., not significant (Student's t-test) **(B)** UCSC Genome Browser shots of m⁶A-IP profiles of RNA isolated from *Mettl3* KO, *Zc3h13* KO and WT cells and input samples for each genetic background at the *Wtap* encoding locus. Scale is mapped reads in 100-bp bins normalized to mean library size. **(C)** Meta plot depicting reads from m⁶A-IP's at target genes (defined as genes overlapping or within 500bps of MACS identified peaks of m⁶A-IP/input in WT cells) aligned to the transcription start site (TSS) and transcription end site (TES). **(D)** LC-MS/MS quantification of m⁶A levels in either control samples or in mRNA extracts depleted for the indicated proteins in S2R+ cells. Bar chart is showing the mean of three biological replicated and three independent measurements; errors bars indicate standard deviation (s.d.). *, $P < 0.01$ (Student's t-test). KD of indicated proteins significantly reduces m⁶A levels. **(E)** Fold enrichment of m⁶A-regulated transcripts (*Aldh-III* and *Dsp1*) over input in Myc-Ythdc1 RNA immunoprecipitation after control or Flacc depletion. Bar chart is showing the mean of three biological replicates; errors bars indicate standard deviation (s.d.). *, $P < 0.01$; **, $P < 0.001$ (Student's t-test). Loss of Flacc affects Ythdc1 binding. **(F)** Relative isoform quantification of m⁶A-regulated genes (*Aldh-III*, *Hairless* and *Dsp1*) upon depletion of indicated components. Flacc is required for m⁶A-dependent splicing events.

Figure 3. Flacc regulates common transcripts with other components of the m⁶A complex.

(A) Number of differentially expressed genes upon KD of indicated proteins (left) and venn diagram of common differentially expressed targets regulated by components of MACOM complex (right). (B) Scatterplot of the first two principal components of a PCA of the 500 most variable genes in all conditions. The biological replicates are indicated in

the same colour, with elliptic areas representing the standard deviation of the two depicted components. (C) Boxplot plots of the gene length distribution for genes tested in the differential expression analysis and the differential expressed genes up- or down-regulated in all conditions. The distributions were tested for difference using the Kolmogorov-Smirnov test. (D) Overlap between common up, down or all differentially expressed genes and m⁶A containing genes (miCLIP data from (Kan et al. 2017b)). The significance of the overlap was tested using a hypergeometric test. (E) Heatmap of the foldchange (log₂) of commonly mis-regulated genes. The heatmap is clustered according to rows and columns. The color gradient was adjusted to display the 1% lowest/highest values within the most extreme color (lowest values as the darkest blue, highest values as the darkest red). (F) The GO term analysis of common common up and down regulated genes, performed using the package ClusterProfiler. Top 10 GO-terms are displayed.

Figure 4. Flacc is required for sex determination via control of *Sex lethal* alternative splicing

(A and B) *domeGAL4* driven expression of shRNA or dsRNA in genital discs and first pair of leg discs against Nito or Flacc respectively. (top) Foreleg of a WT male and female flies depleted for Nito or Flacc show appearance of male specific sex comb bristles (red arrow). (below) Depletion of Nito or Flacc results in transformations of female genitalia and loss of vaginal bristles (red arrowhead). **(B)** Quantification of female survival and transformations in escapers upon depletion of Nito or Flacc using *DomeGAL4* driver. *n* – number of analysed flies with the expected number of escapers in brackets. Depletion of Nito and Flacc results in high level of transformation in female genitalia and appearance of male specific sex combs on forelegs. **(C)** Semi-quantitative

RT-PCR analysis of *Sxl* isoforms in male and female heads from flies depleted for Fl(2)d, Nito or Flacc respectively using *Elav*GAL4 driver. Inclusion of male specific exon L3 is observed in flies lacking m⁶A components. **(D)** *flacc* locus (*flacc*^C) with premature stop codon at amino acid Leu730. Sites of dsRNA fly lines KK110253 and GD35212 are shown below gene loci. **(E)** Viability of female flies from a cross of indicated genotypes mated with *Sxl*^{7BO} males. Loss of one copy of *flacc* significantly reduces female survival in a genetic background where one copy of *Sxl* and *da* are absent. The same compromised survival is observed for other m⁶A components (*Mettl3*, *Mettl14*, *Ythdc1*, *fl(2)d*, *vir* and *nito*). **(F)** Viability of female flies with homozygous *vir2F* mutation can be rescued by loss of single copy of *flacc* and *nito*.

Figure 5. Flacc bridges the methyltransferase complex to mRNA targets via binding to Nito

(A) Co-immunoprecipitation experiments were carried out with lysates prepared from S2R+ cells, transfected with GFPMyC-Nito and Fl(2)d-HA. In control lanes, S2R+ cells were transfected with Myc alone and identical HA-containing protein. Extracts were immunoprecipitated with Myc antibody and immunoblotted using Myc and HA antibodies. 2% of input was loaded. The same experiment was repeated in Flacc KD condition. Interaction between Nito and Fl(2)d is strongly reduced upon depletion of Flacc. **(B)** Fold enrichment of m⁶A-regulated transcripts (*AldhIII*, *Hairless*, *Dsp1*) over input in Myc-Fl(2)d and Myc-Nito RNA immunoprecipitation upon depletion of Flacc or in control condition. Bar chart is showing the mean of three biological replicates; errors bars indicate standard deviation (s.d.). *, P<0.01; **, P<0.001; ***, P<0.0001 and n.s., not significant (Student's t-test). Loss of Flacc strongly affects Fl(2)d binding and to milder extent binding of Nito to m⁶A regulated transcripts. **(C and D)** Co-

immunoprecipitation experiments were carried out with lysates prepared from S2R+ cells, transfected with either FlagMyc-Nito and Fl(2)d-HA. In control lanes, S2R+ cells were transfected with FlagMyc alone and identical HA-containing protein. Extracts were immunoprecipitated with Flag antibody and immunoblotted using Myc and HA antibodies. 2% of input was loaded. The same experiment was performed upon depletion of Flacc. Human ZC3H13 was transfected in identical set of experiment. Interaction between Nito and Fl(2)d is strongly reduced upon loss of Flacc (lane 6), but can be rescued upon expression of human ZC3H13 protein (lane 8). Quantification of two replicates is shown in (D).

Figure 6. Zc3h13 stabilized the interaction between RBM15 and WTAP

(A and B) Comparison of TAP-LC-MS/MS of endogenously FLAG-Avi tagged Rbm15 mESC's in either a WT or *Zc3h13* KO background. Rbm15 and associated proteins were purified in the presence of 350mM NaCl. **(A)** Volcano plot showing enriched proteins in WT cells (right) vs *Zc3h13* KO cells. **(B)** Table of spectral counts, unique peptides and % coverage of TAP-LC-MS/MS data in (A). **(C)** Split luciferase NanoBiT assay examining the interaction of mouse Rbm15 and Wtap. Left, scheme representing Luciferase reconstitution upon transfection of LgBit and SmBit NanoLuc subunit fusions and interaction of Rbm15 and WTAP. Right, comparison of Rbm15-Wtap NanoBiT NanoLuc signal in WT, *Zc3h13* and *Mettl3* KO cells. Mean of three independent experiments, three transfections each; errors bars indicate standard deviation (s.d.). * $P=0.026$, calculated using two-tailed Student's *t*-test.

Figure 7. Schematic Representation of the role of MACOM and MAC complexes..

MACOM complex can regulate gene expression in two ways; either on its own (MAC independent functions) or by interacting with MAC components (m⁶A methylation). Flacc (Zc3h13) is a novel component of the MACOM complex that stabilizes the interaction between Fl(2)d and Nito (WTAP and RBM15) proteins, thereby ensuring deposition of m⁶A to targeted transcripts.

Supplemental Figure 1. Generation of tagged and knock-out mESC lines

(A) Schematic of CRISPR/Cas9 strategy to endogenously N-terminally tag Rbm15 and Mettl3 in mESCs expressing the bacterial *BirA* ligase. A ssODNA with homology arms was used as donor to integrate the tag. (B) Western blot confirmation of clones expressing FLAG-Avi Tagged Rbm15 and Mettl3. For Rbm15, presence of tagged protein was verified by probing a membrane with streptavidin coupled HRP (left); the Mettl3 membrane was probed with anti-Flag antibody as mESCs express an endogenously biotinylated protein of circa. 70Kd (right). (C) Scheme of CRISPR/Cas9 strategy to ablate Zc3h13. Two independent sgRNAs guide Cas9 to remove exons 9 and 10 resulting in a non-functional truncated protein. Western blot of Zc3h13 to confirm deletion (below).

Supplemental Figure 2. Flacc/Zc3h13 regulates the m⁶A pathway, supporting data I

(A) TAP-LC-MS/MS of endogenously FLAG-Avi tagged Mettl3 mESC's compared to Parental untagged in presence of 150mM NaCl. Highlighted are enriched proteins (red) including novel protein Zc3h13 (green). (B) iBAQ values for selected proteins for (A).

Supplemental Figure 3. Flacc/Zc3h13 regulates the m⁶A pathway, supporting data II

(A and B) Co-immunoprecipitation experiments were carried out with lysates prepared from S2R+ cells, transfected with FlagMyc-Flacc and HA-Fl(2)d (A) or HA-Vir (B). In control lanes, S2R+ cells were transfected with FlagMyc alone and identical HA-containing protein. Extracts were immunoprecipitated with Myc antibody and immunoblotted using Flag and HA antibodies. 2% of input was loaded. The same experiment was repeated in the presence of RNaseT1. Fl(2)d and Vir interact with Flacc in an RNA independent manner. (C and D) Western blot validation of RNA immunoprecipitation experiments, which were carried out with lysates prepared from

S2R+ cells, transfected with GFPMyC-tagged control, Fl(2)d, Nito and Ythdc1 constructs. Extracts were immunoprecipitated with Myc antibody and immunoblotted using Myc antibody. 2% of input was loaded. The same experiment was performed upon Flacc depletion. Relative expression of *flacc* levels is shown in (D).

Supplemental Figure 4. Phylogenetic characterization of ZC3H13 proteins.

(A) Phylogenetic tree of the full sequence alignment of orthologs of ZC3H13 in 23 species. The labels indicate the gene names (from the NCBI's Entrez database) and the abbreviated species name. (B) N-terminal part of the multiple sequence alignment used to construct the phylogenetic tree, including the zinc-finger (boxes). (C) Tree of the 23 species included in the phylogenetic analyses. Coloring indicates whether the indicated taxa or species contain a ZC3H13 ortholog, and whether the ortholog has the zinc finger or not. The names of 15 species are displayed. The vertebrates included, whose names were not displayed, were: *Danio rerio*, *Callorhinchus milii*, *Latimeria chalumnae*, *Anolis carolinensis*, *Ornithorhynchus anatinus*, *Gallus gallus*, *Mus musculus* and *Homo sapiens*. See methods for details.

Supplemental Figure 5. Flacc regulates common transcripts with other components of the m⁶A complex, supporting data I

(A) Relative expression of indicated transcripts upon control (LacZ), Mettl3, Mettl14, Vir, Nito and Flacc KD. The mean standard deviation of three technical measurements from three biological replicates is shown. (B) Boxplots of average expression (rpkm) for all genes expressed by at least 1 rpkm in the different conditions. The black dots indicate the position of m⁶A components in comparison to other expressed genes. (C) Relative expression of indicated transcripts upon control (LacZ) and Flacc KD. (D) WB for Mettl3,

Mettl14 and Fl(2)d in control (LacZ) and Flacc KD. (E) (A) Relative isoform quantification of m⁶A-regulated genes (*CG8929*, *dorsal*, *fl(2)d*) upon depletion of indicated components. Flacc is required for m⁶A-dependent splicing events.

Supplemental Figure 6. Flacc regulates common transcripts with other components of the m⁶A complex, supporting data II

(A) Number of differentially spliced genes upon KD of indicated proteins. (B) Distribution of splicing events in the different KD conditions. The pie chart for “Control” depicts the detected splice events on average in all the comparisons “control vs. KD”. The pie charts for the individual KD depict the amount of significantly different splicing events with a FDR value below 10%. Intron retention and alternative 5`splice site usage are over-represented upon KD of m⁶A components. (C) Overlap between common differentially spliced genes and m⁶A containing genes (miCLIP data from (Kan et al. 2017)). The significance of the overlap was tested using a hypergeometric test. Common differentially spliced genes are highly methylated. (D) Venn diagrams of common differentially spliced events regulated by components of MACOM complex (E) The GO term analysis of common differentially spliced genes, performed using the package ClusterProfiler. Top 10 GO-terms are displayed.

Supplemental Figure 7. Flacc sub-cellular localization and expression through development

(A) Immunostaining of Myc-tagged Flacc protein in S2R⁺ cells. GFP-tagged Barentsz was used as a cytoplasmic marker. Scale bar, 5 μ m. (B) *in situ* RNA hybridization of *flacc* (*flacc-as*), *flacc* control (*flacc-s*), *elav* positive control (*elav-as*) and *elav* negative control (*elav-s*) are shown. Scale bars, 100 μ m. (C) Relative *flacc* mRNA expression and levels

of m⁶A in mRNA during *Drosophila* development. Number of hours post-fertilization for different embryo, larval and pupal stages is indicated below. The mean with standard deviation of three technical measurements from three biological replicates is shown. **(D)** Relative expression of indicated transcripts in fly heads upon control, Fl(2)d, Nito or Flacc KD. The mean standard deviation of three technical measurements from two biological replicates is shown.

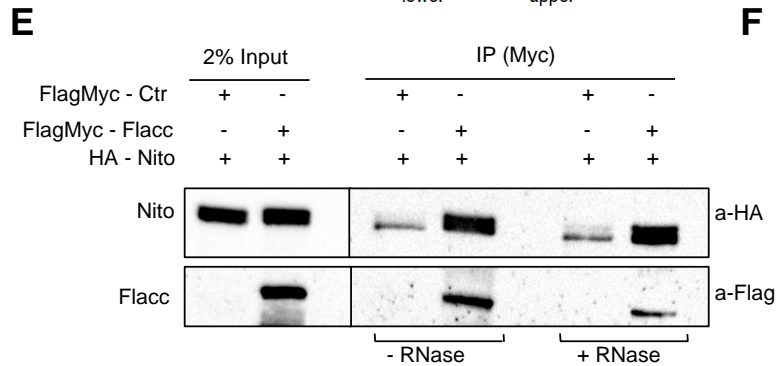
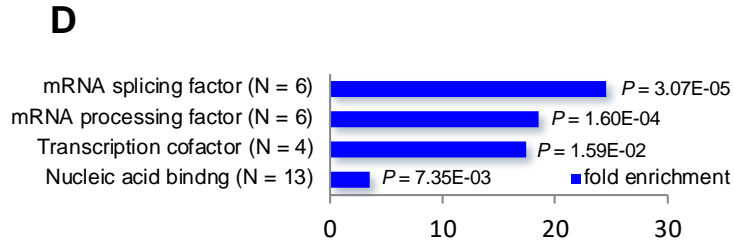
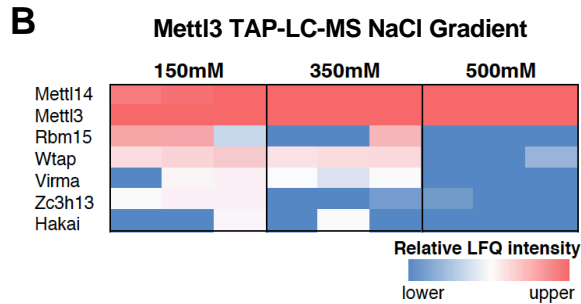
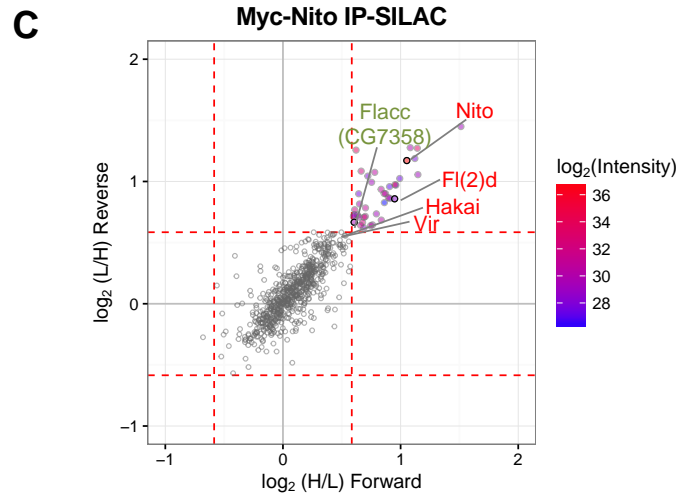
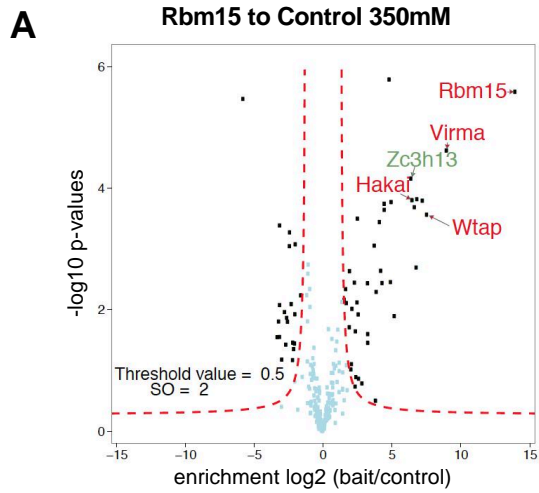
Supplemental Figure 8. Flacc depletion does not interfere with interactions between two methyltransferases or between Vir and Fl(2)d.

(A-F) Co-immunoprecipitation experiments were carried out with lysates prepared from S2R⁺ cells, transfected with either GFPMyC-Mettl3 and Mettl14-HA (A), or Myc-Nito and Vir-HA (C), or Myc-Fl(2)d short isoform, Myc-Fl(2)d long isoform and Vir-HA (E). In control lanes, S2R⁺ cells were transfected with GFPMyC alone and identical HA-containing proteins. Extracts were immunoprecipitated with Myc antibody and immunoblotted using Myc and HA antibodies. 2% of input was loaded. The same experiments were performed upon depletion of Flacc. Interactions between Mettl3 and Mettl14, and Fl(2)d and Vir do not depend on the presence of Flacc (A, C and E). Relative expression of *flacc* levels is shown in (B, D and F). Star indicates IgG band in figure (A). **(G and H)** Co-immunoprecipitation experiments were carried out with lysates prepared from S2R⁺ cells, transfected with either FlagMyC-Nito and Mettl3-HA (A), or FlagMyC-Nito and Mettl14-HA (C). In control lanes, S2R⁺ cells were transfected with GFPMyC alone and identical HA-containing proteins. Extracts were immunoprecipitated with Myc antibody and immunoblotted using Myc and HA antibodies. 2% of input was loaded. The same experiments were performed upon depletion of Flacc. Interactions

between Nito and Mettl3/Mettl14 are not affected by depletion of Flacc. **(I)** Related to Figure 5A. Relative levels of *flacc* in indicated samples. The mean with standard deviation of three technical measurements is shown. **(J and K)** Related to Figure 5C. Relative levels of human ZC3H13 transfected in indicated samples (J) and Relative levels of *flacc* in indicated samples (K). The mean with standard deviation of three technical measurements from two biological replicates is shown.

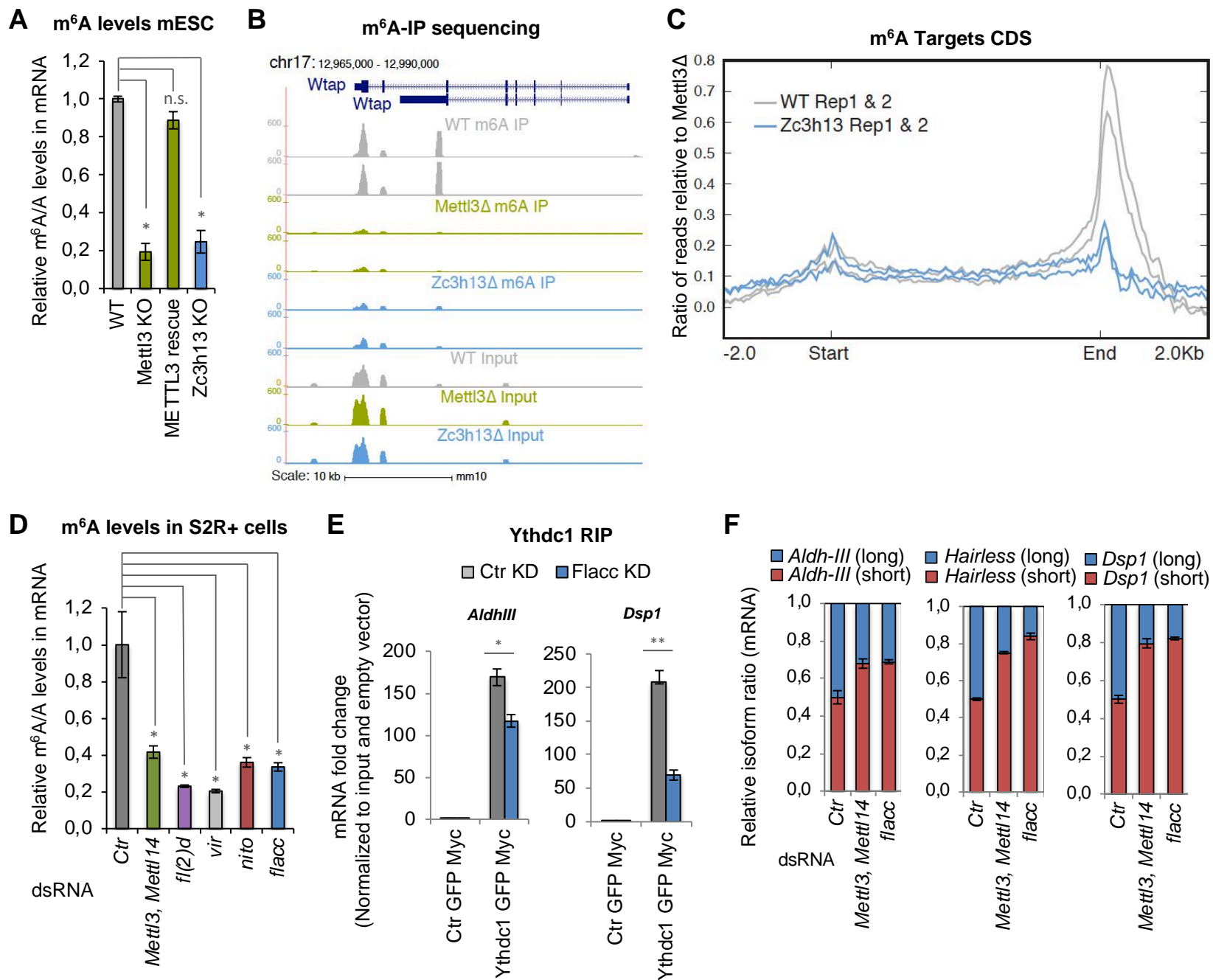
Supplemental Figure 9. Zc3h13 stabilizes the interaction between Rbm15 and Wtap.

(A and B) Comparison of TAP-LC-MS/MS of endogenously FLAG-Avi tagged Rbm15 mESC's in either a WT or *Zc3h13* KO background. Rbm15 and associated proteins were purified from nuclear fractions of lysates. (A) Volcano plot showing enriched proteins in WT cells (right) vs *Zc3h13* KO cells. (B) Table of spectral counts, unique peptides and % coverage of TAP-LC-MS/MS data in (A). **(C)** Western blot analysis comparing WT to *Zc3h13* KO mESCs levels of Rbm15, Mettl3, Wtap and Hakai, Tubulin was used as loading control). * Denotes shift in Rbm15 due to Flag-Avi tag. **(D)** Split luciferase NanoBiT assay examining mouse Rbm15 and Wtap. Scheme depicting example fusion constructs generated to determine optimal configuration of fusion proteins. e.g. Wtap-C-Ig is C-terminally tagged Wtap fused to the large subunit of NanLuc. **(E)** Luciferase assays comparing all possible LgBit and SmBit NanoLuc subunit fusions to Rbm15 and Wtap to determine which combination provides the strongest signal. **(F)** RT-qPCR measurements of WT-N-sm and Rbm15-C-Ig fusion constructs in WT, *Zc3h13* and *Mettl3* backgrounds.



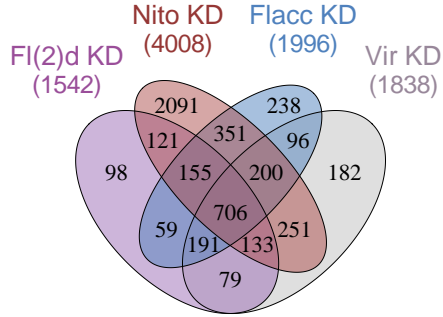
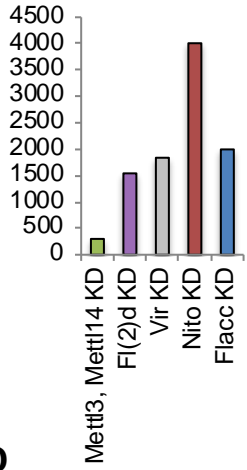
F

<i>M. musculus</i>	<i>D. melanogaster</i>	Complex
Mettl3	Mettl3 (CG5933)	"MAC" m ⁶ A-METTL Complex
Mettl14	Mettl14 (CG7818)	
Rbm15	Nito (CG2910)	"MACOM" m ⁶ A-METTL Associated Complex
Wtap	FI(2)d (CG6315)	
Virma	Vir (CG3496)	
Zc3h13	Flacc (CG7358)	
Hakai	Hakai (CG10263)	

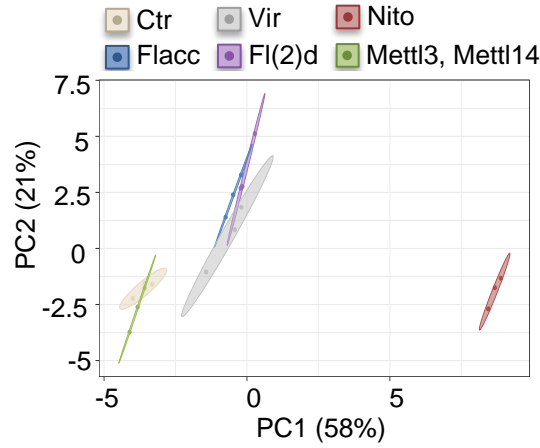


A

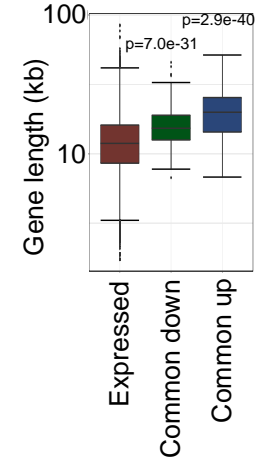
Differentially expressed genes (n)



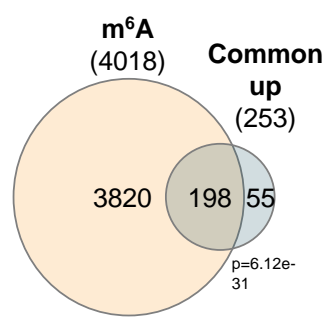
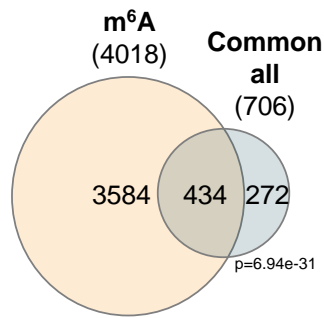
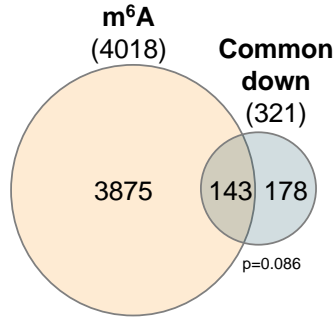
B



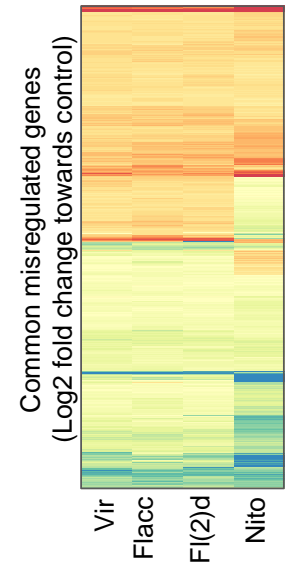
C



D

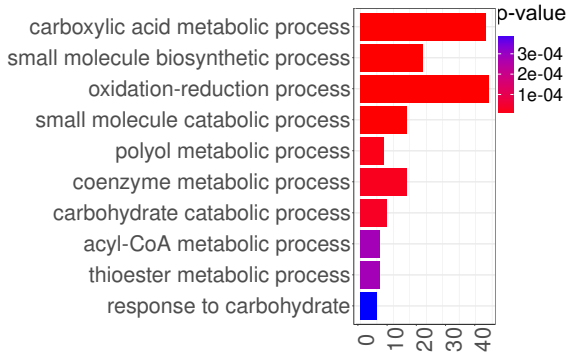


E

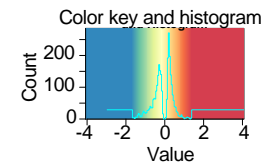
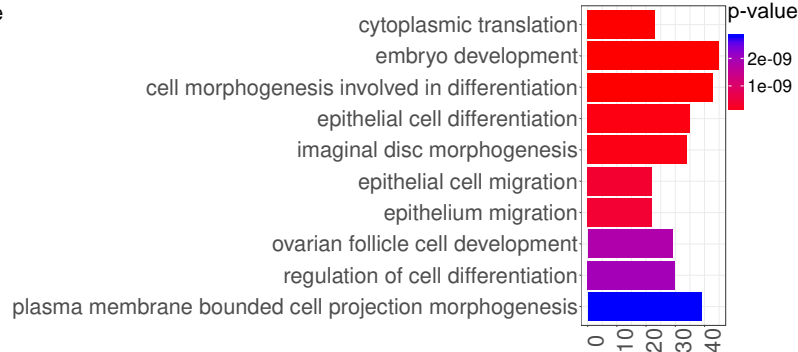


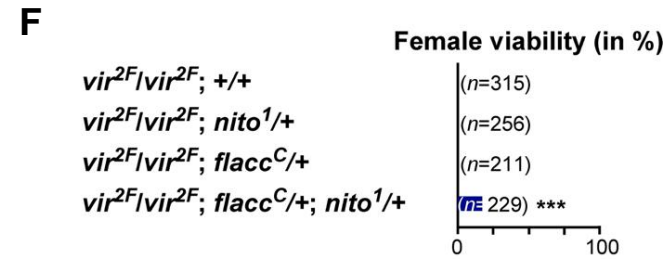
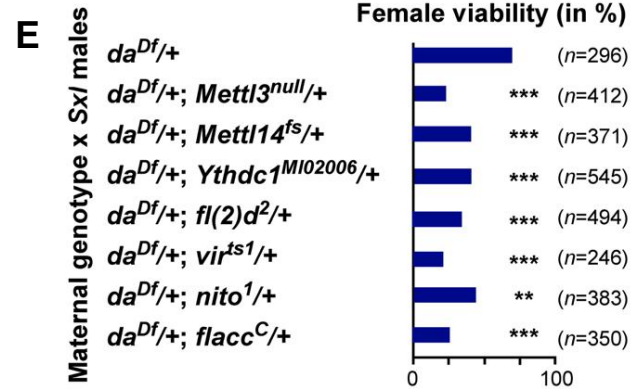
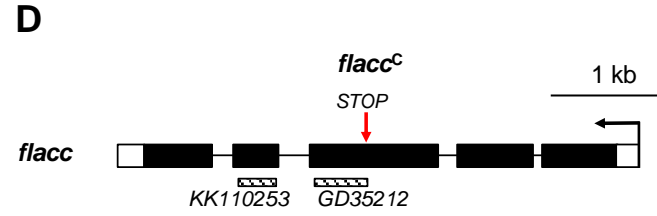
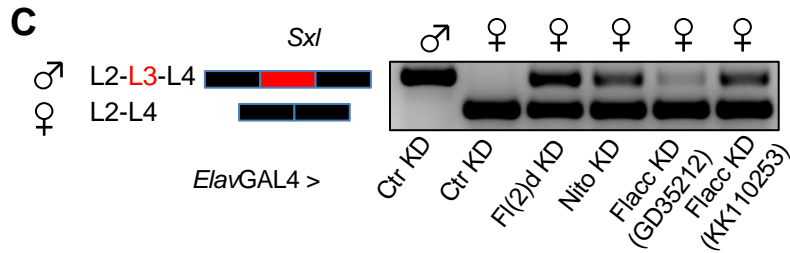
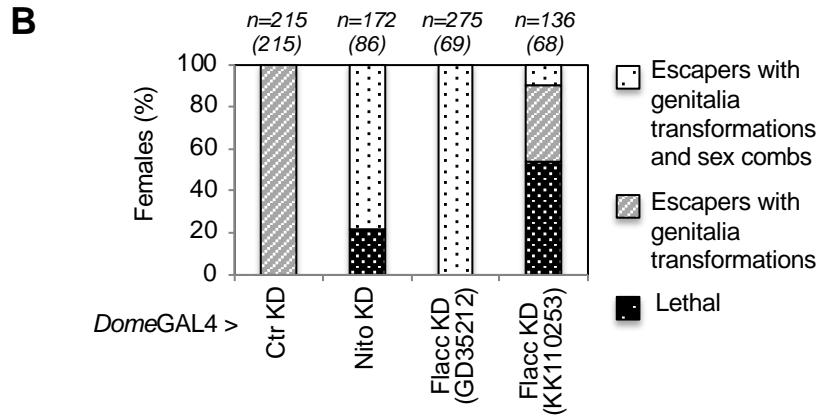
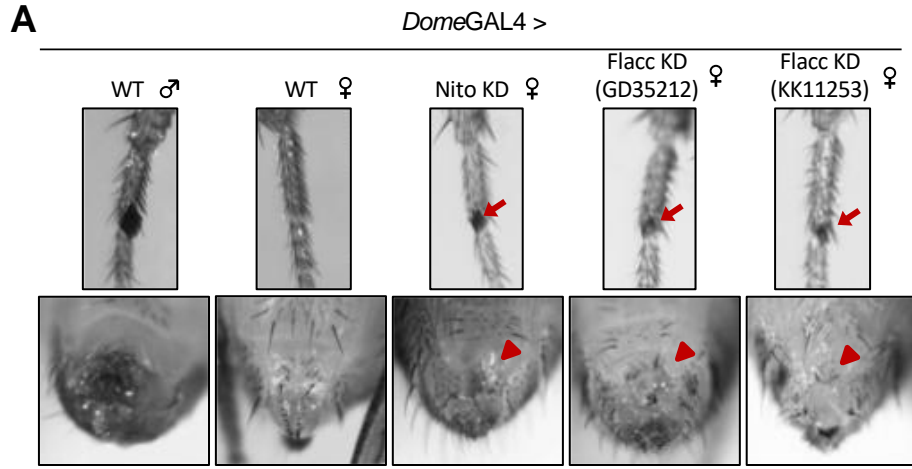
F

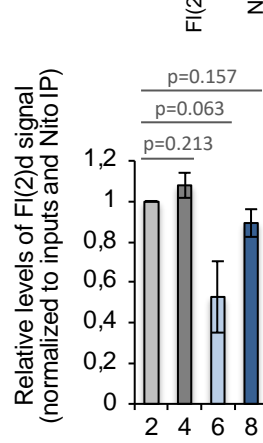
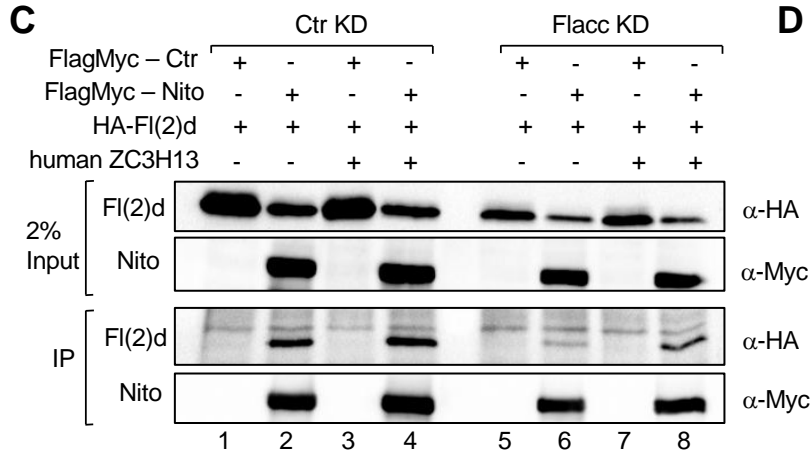
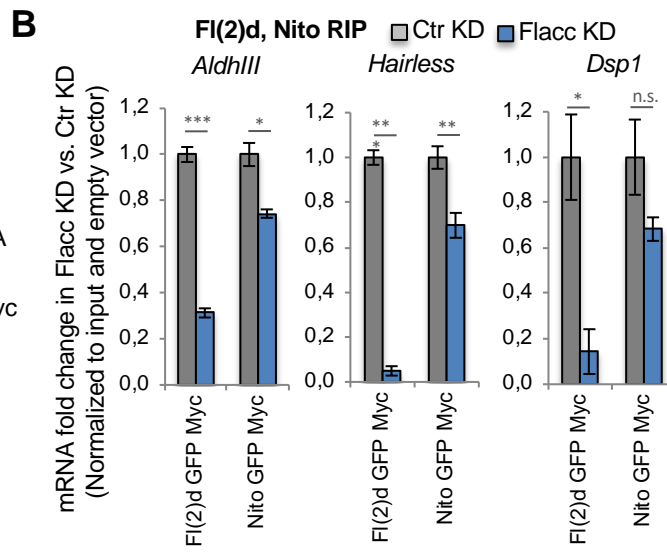
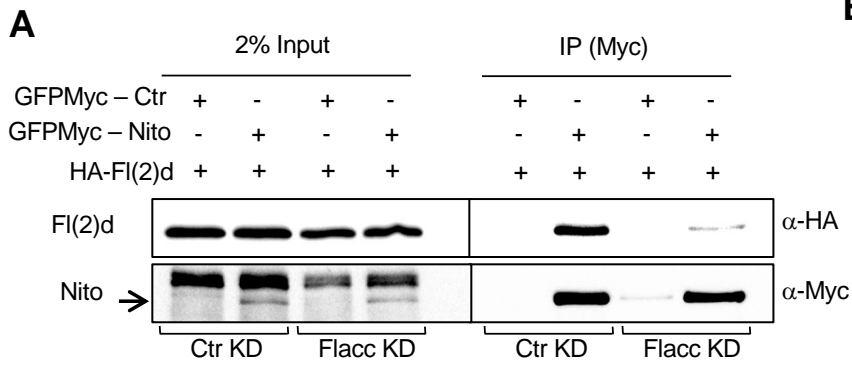
Enriched terms (Common down)



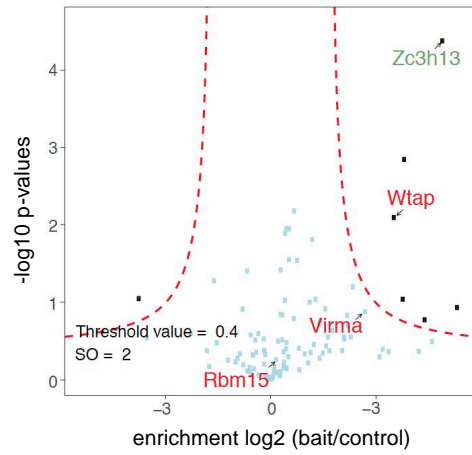
Enriched terms (Common up)







A Rbm15 WT to Rbm15 in *Zc3h13*KO

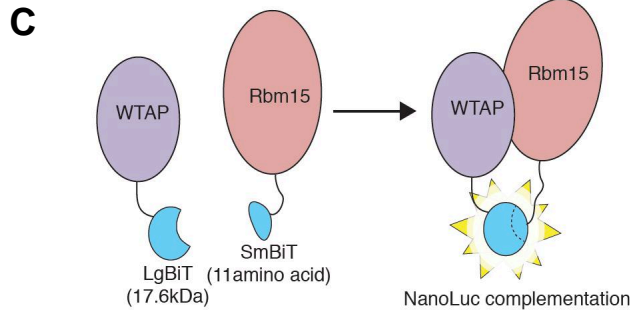
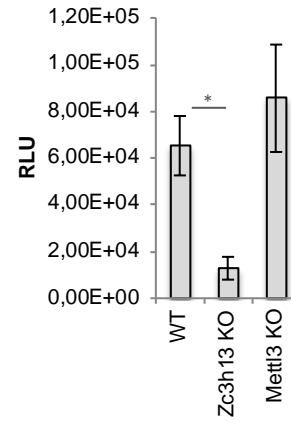


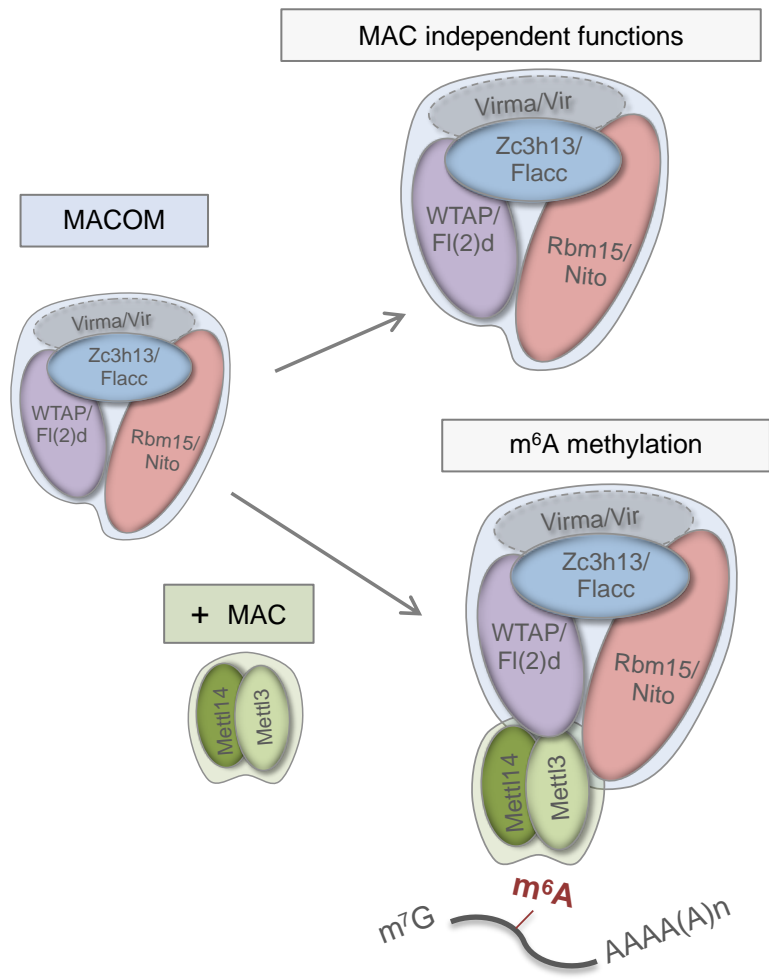
B Rbm15 IP-LC-MS from whole cell extracts

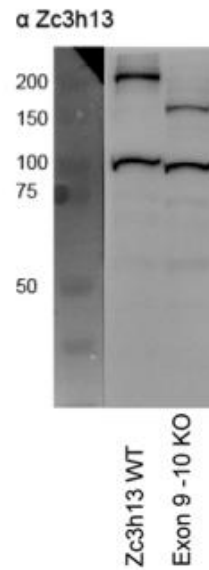
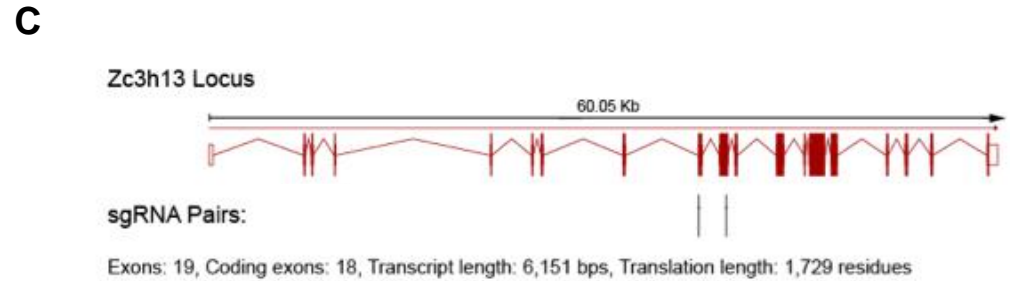
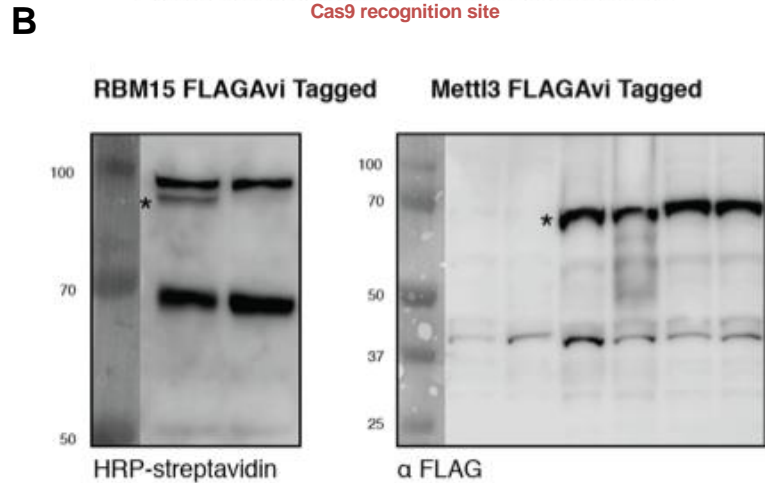
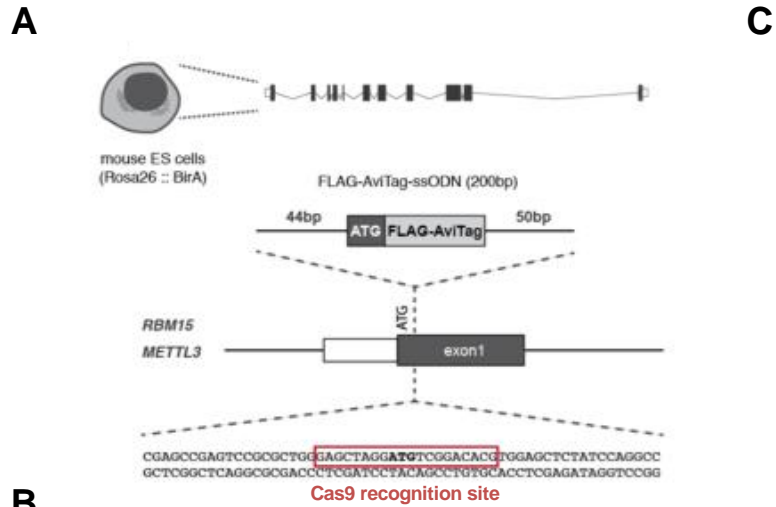
	Untagged	WT	<i>Zc3h13</i> <i>-/-</i>
Rbm15	- / - / -	566 / 51 / 49%	652 / 56 / 54%
Wtap	- / - / -	29 / 5 / 20%	4 / 3 / 8.1%
Virma	- / - / -	8 / 3 / 2.4%	1 / 1 / 0.7%
Zc3h13	- / - / -	6 / 1 / 0.8%	- / - / -

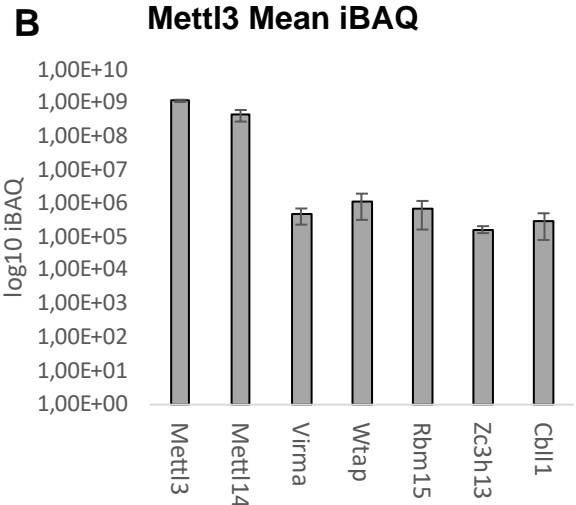
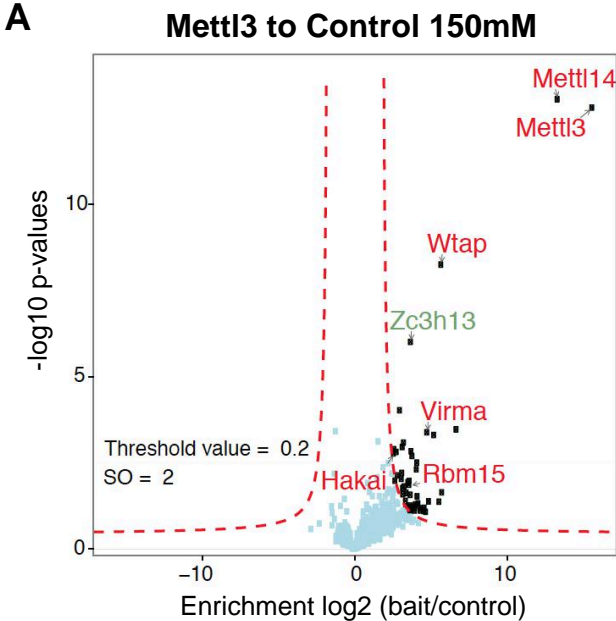
total spectrum count/ total unique peptide count/ % sequence coverage

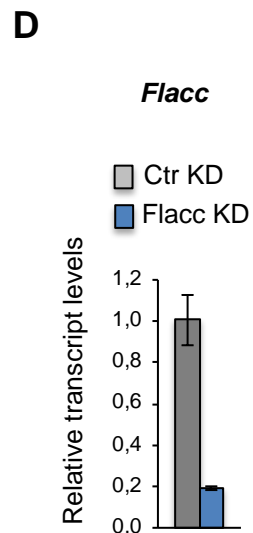
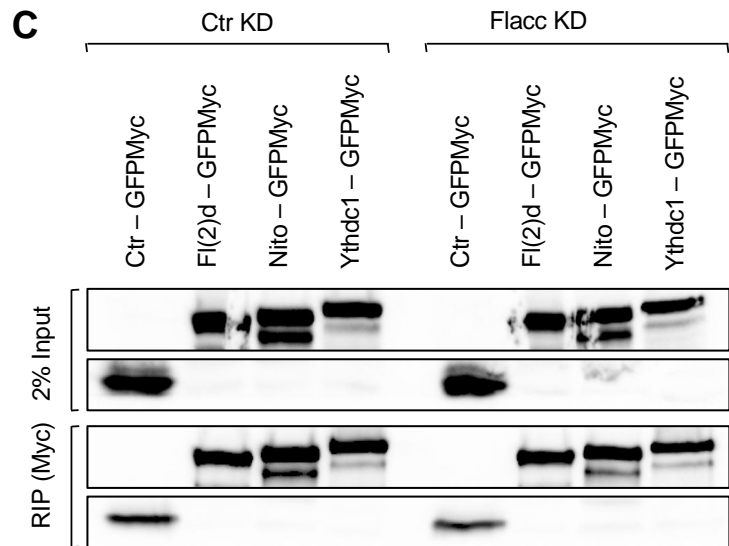
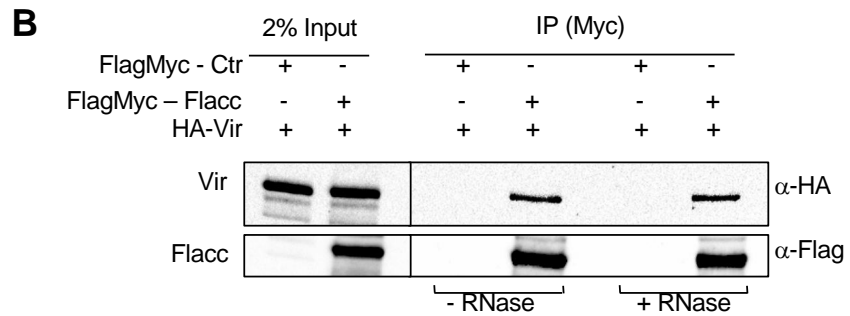
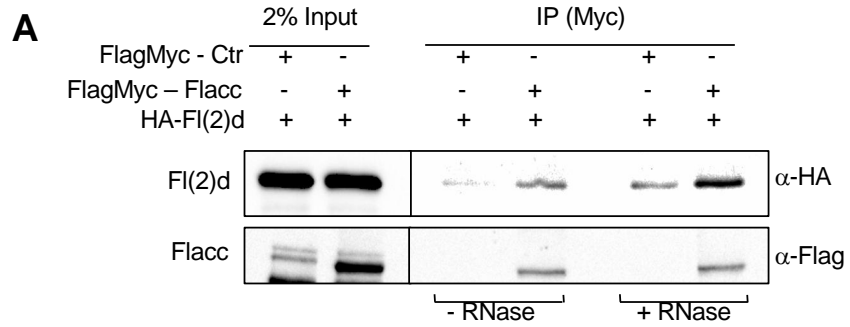
Rbm15-Wtap NanoBiT

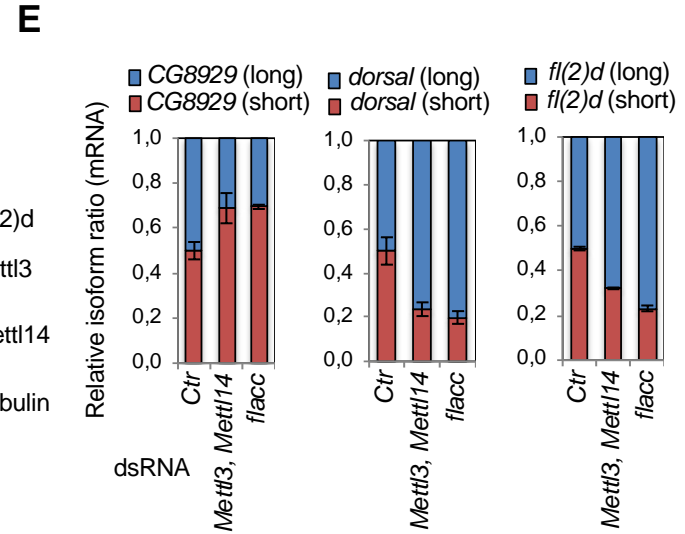
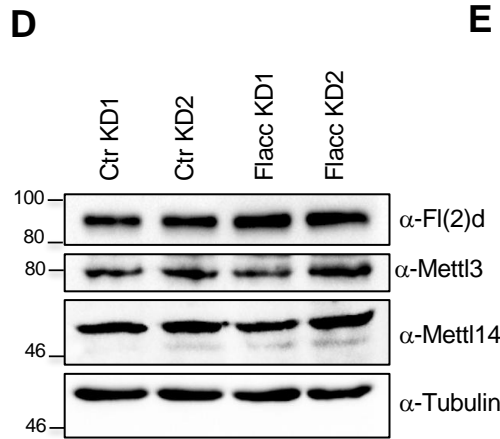
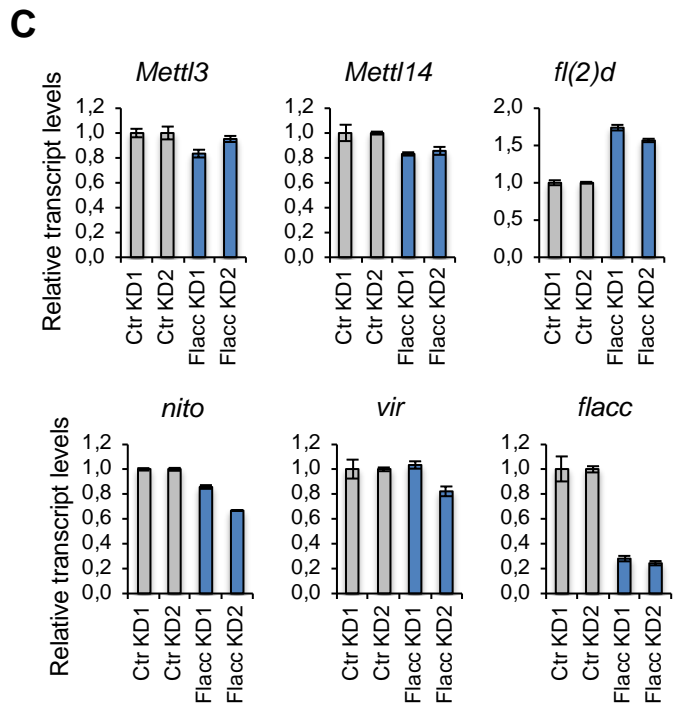
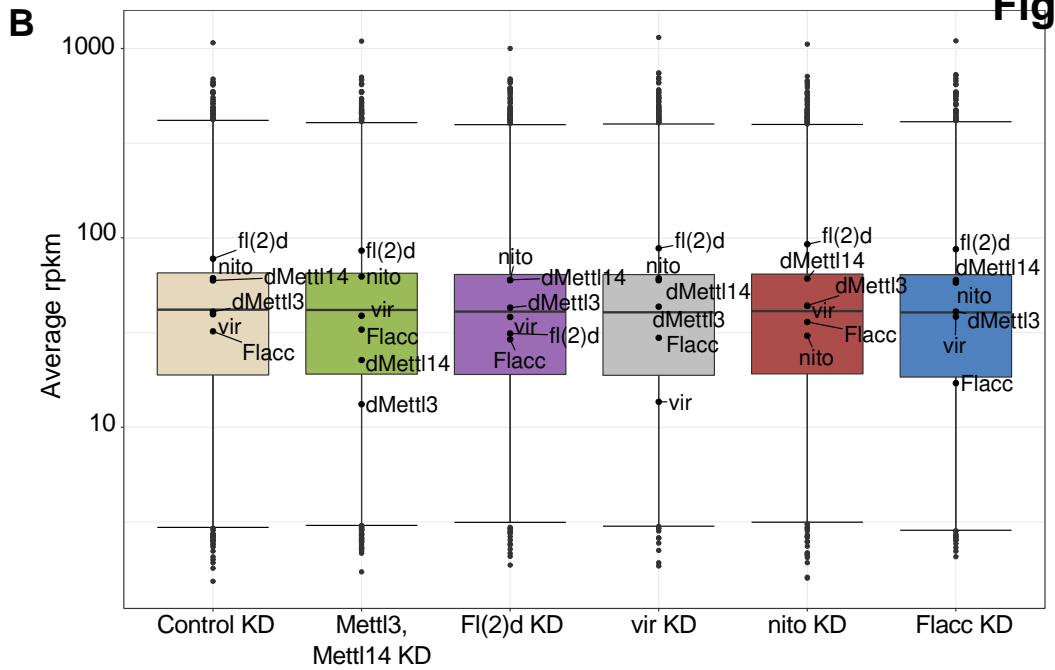
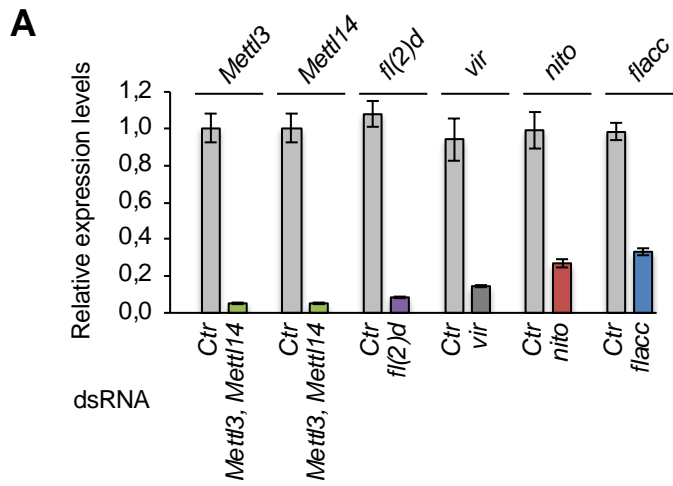


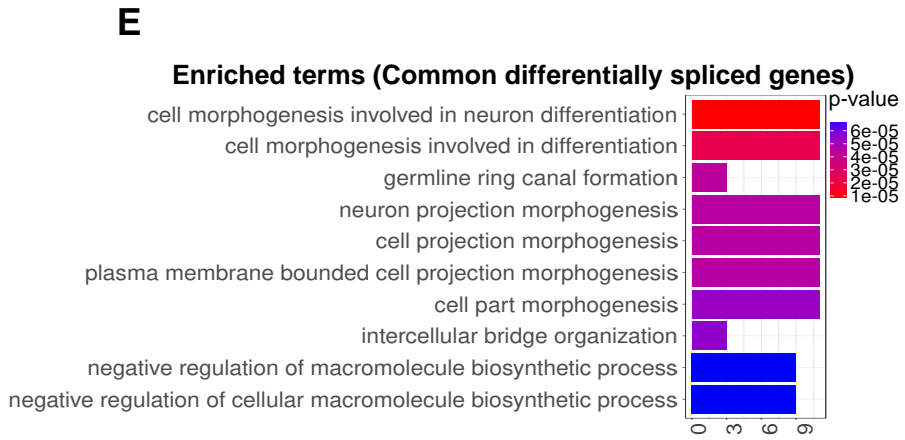
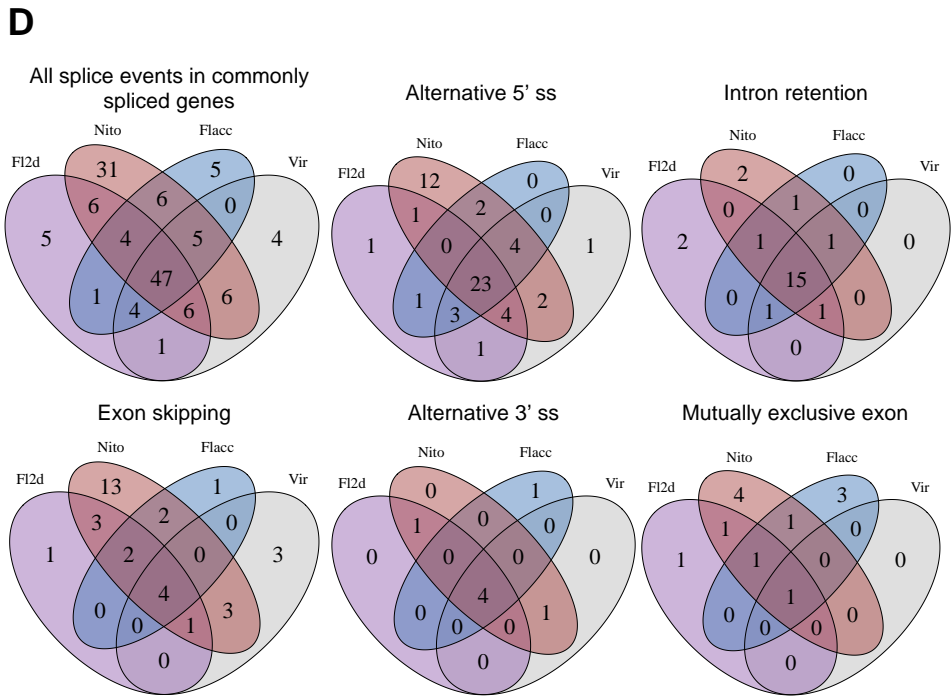
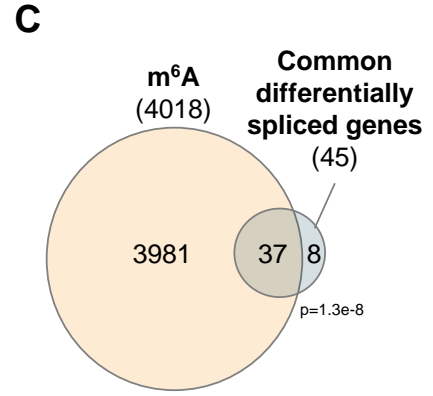
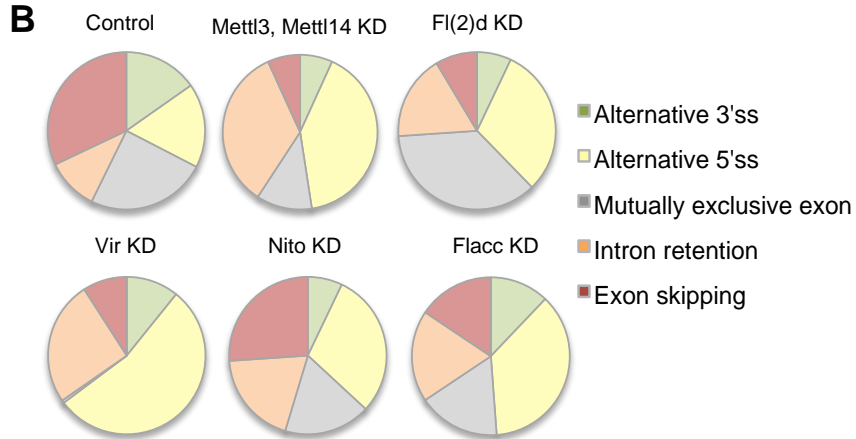
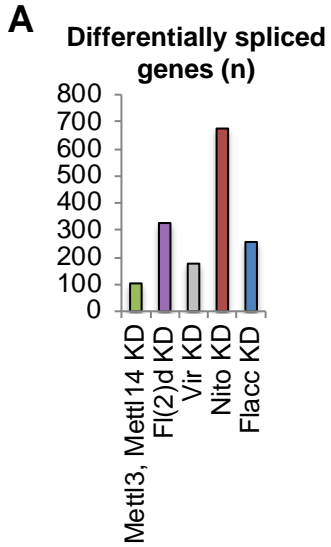




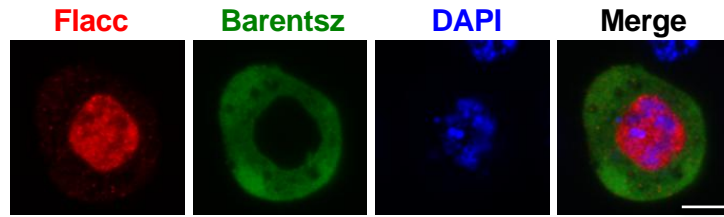




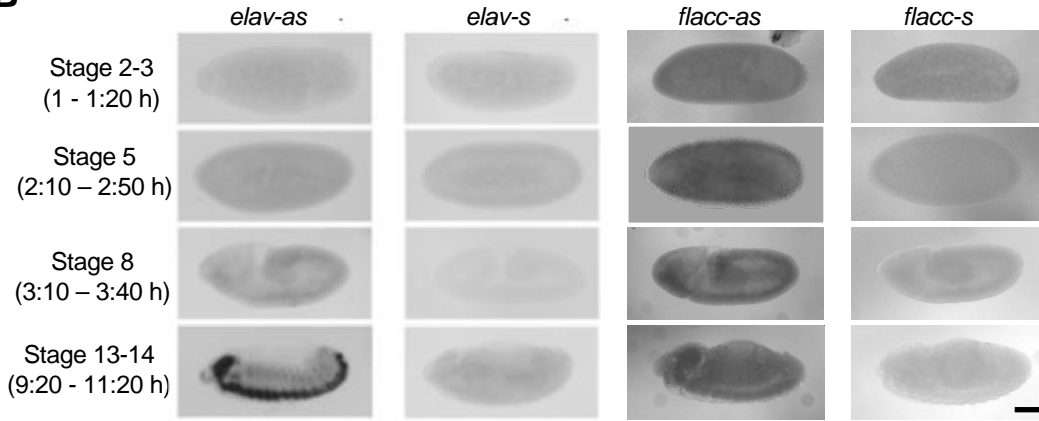




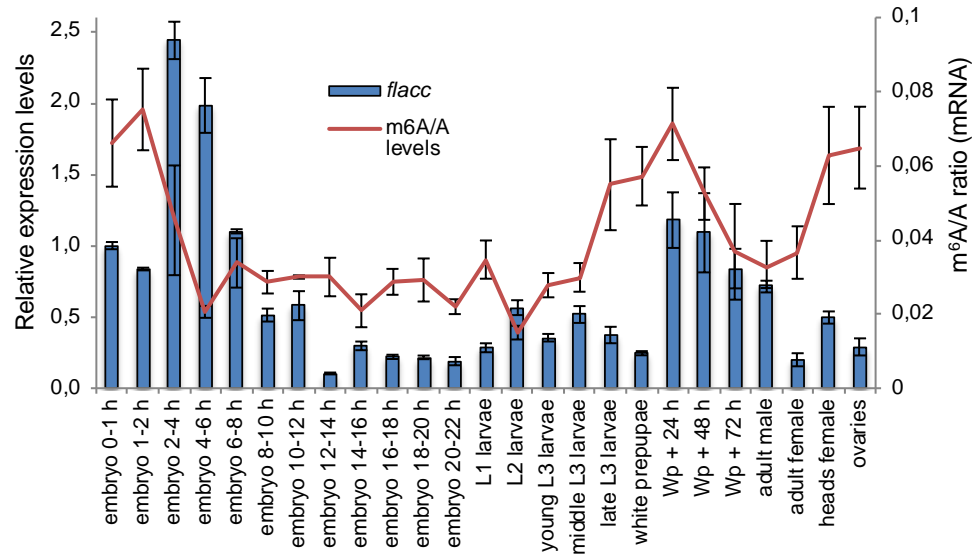
A



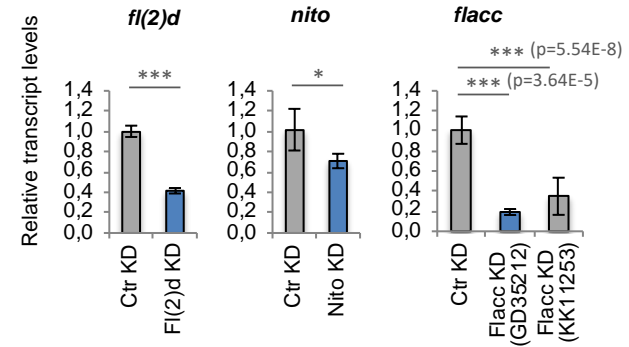
B

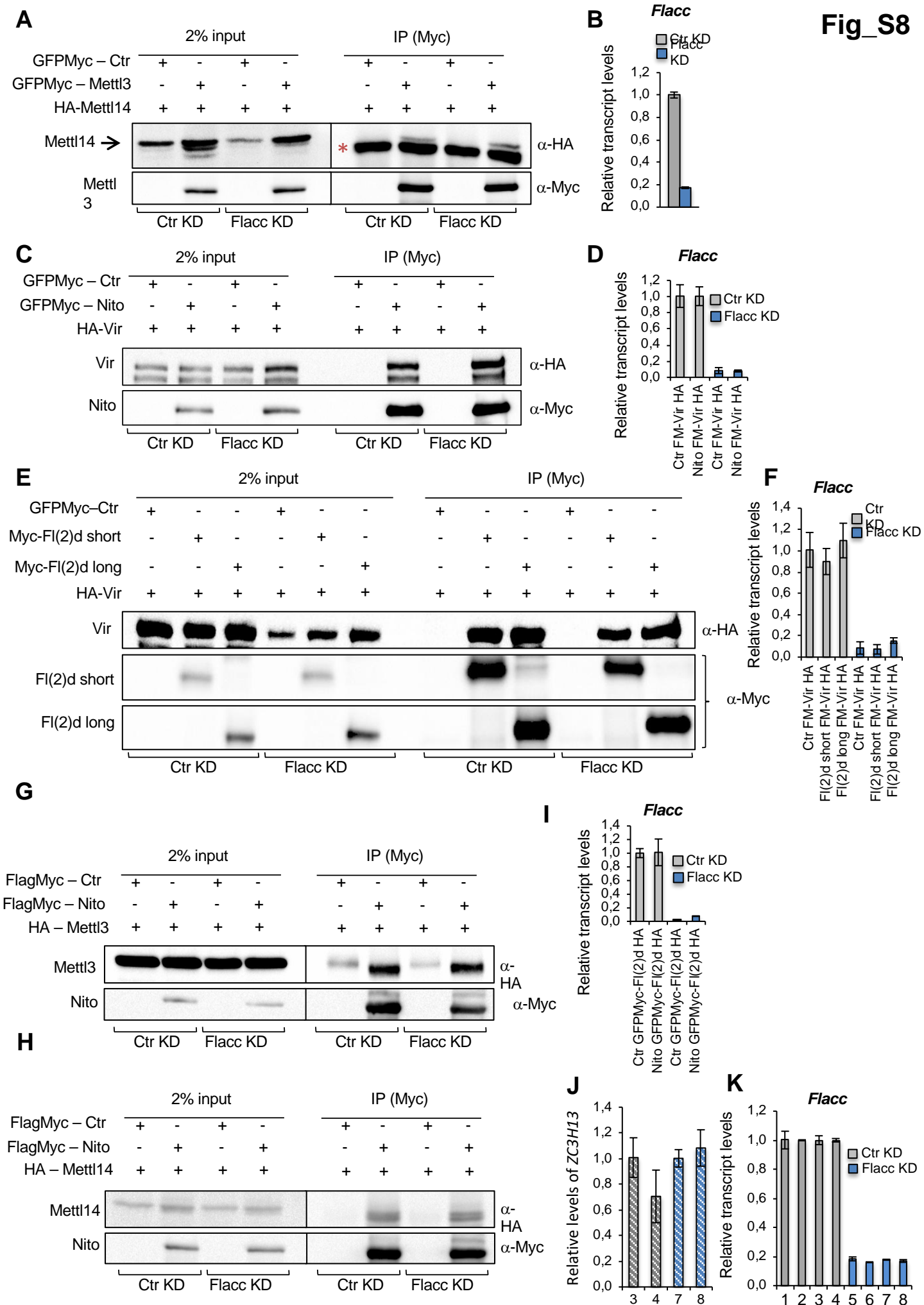


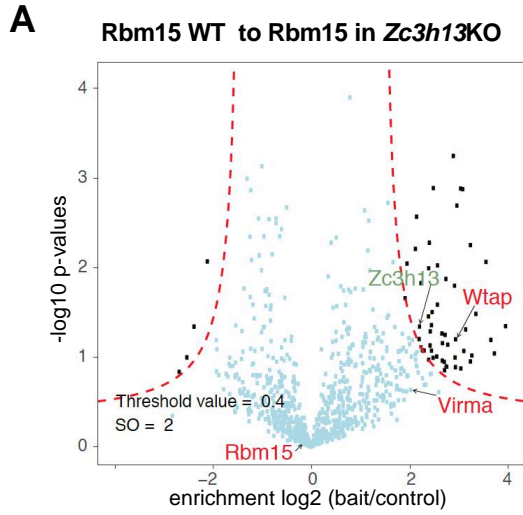
C



D







B Rbm15 IP-LC-MS from nuclear fraction

	Untagged	WT	<i>Zc3h13</i> <i>-/-</i>
Rbm15	8 / 2 / 3.6%	356 / 27 / 35%	340 / 29 / 30%
Wtap	- / - / -	25 / 6 / 20%	1 / 1 / 2.3%
Virma	- / - / -	20 / 4 / 3%	1 / 1 / 1.1%
<i>Zc3h13</i>	- / - / -	5 / 1 / 1.6%	- / - / -

total spectrum count/ total unique peptide count/ % sequence coverage

